

## E.02.18 – ELSA

# D2.4 – SESAR Agent Based Model

Document information	
Project title	Empirically grounded agent based models for the future ATM scenario
Project N°	E.02.18.
Project Manager	Deep Blue
Deliverable Name	SESAR Agent Based Model
Deliverable ID	D2.4
Edition	00.00.04
Template version	02.00.00
Task contributors	
C. Bongiorno, S. Miccichè [UNIPA], G. Gurtner, M. Ducci, S. Pozzi [Deep Blue]	

### Abstract

This document is the deliverable D2.4 “SESTAR Agent Based Model” describing the Agent Based Model developed within the extension of the ELSA project. The deliverable describes the different modules of the model and the way numerical simulations have been implemented. We performed numerical simulations with the aim of showing how the different modules of the model can work. Therefore, the results illustrated in the results section must be intended as indicative of the model’s capabilities.

In the first chapter we describe the model’s objectives and its different modules that try to implement them. The model in its present form shares its main features with the tactical layer of the Agent based Model already presented in deliverable D2.3.

In the second chapter we present the activities that we have conducted in order to calibrate some of the model’s parameters and to validate its main assumptions with the help of SESAR experts and ATC controllers.

In the third chapter we describe the ABM modules that provide the input data to the model. In fact, we have two modules: one that works on real M1 files and does not take into account capacity constraints and the second that works on fully surrogate data and considers sectors capacities. This last module is essentially based on the strategic layer of the ABM presented in deliverable D2.3, thus realizing the objective of integrating the strategical and the tactical layer of the model presented in D2.3.

In the fourth chapter we illustrate the model capabilities by performing a few simulation experiments.

## Authoring & Approval

### Prepared By

Name & company	Position / Title	Date
Salvatore Miccichè (UNIPA)	Assistant Professor of Applied Physics	23/03/2015
Christian Bongiorno (UNIPA)	Fellow holder	23/03/2015
Gérald Gurtner (DBL)	Senior Consultant	23/03/2015
Marco Ducci (DBL)	Validation Expert	23/03/2015

### Reviewed By

Name & company	Position / Title	Date
Marco Ducci (DBL)	Validation Expert	27/03/2015

### Approved By

Name & company	Position / Title	Date
Simone Pozzi (DBL)	Project leader	30/03/2015

## Document History

Edition	Date	Status	Author	Justification
00.00.01	13/03/2015		Salvatore Miccichè	First draft version
00.00.02	17/03/2015		Salvatore Miccichè	Second draft version
00.00.03	23/03/2015		Salvatore Miccichè	Proposed final version
00.00.04	27/03/2015		Salvatore Miccichè	Revised final version
00.00.05	09/06/2015		Salvatore Miccichè	Final version after officers comments

## IPR (foreground)

Foreground owned by the ELSA consortium.

founding members



Avenue de Cortenbergh 100 | B- 1000 Bruxelles | [www.sesarju.eu](http://www.sesarju.eu)

# Contents

DISCLAIMER . . . . .	9
INTRODUCTION . . . . .	10
EXECUTIVE SUMMARY . . . . .	11
<b>1 Model</b>	<b>13</b>
1.1 General features of the model . . . . .	13
1.2 Implementation of the Model . . . . .	15
1.2.1 Time-step choice . . . . .	15
1.2.2 Velocity Noise Module . . . . .	15
1.2.3 Navigation Points . . . . .	16
1.2.4 Flight List module . . . . .	16
1.2.5 Conflict Detection module . . . . .	17
1.2.6 Conflict Resolution module . . . . .	18
1.2.7 Directs module . . . . .	20
1.2.8 Shocks module . . . . .	21
1.2.9 Multi-Sector module . . . . .	22
1.2.10 Model's parameters . . . . .	23
1.3 SESAR scenario trajectories . . . . .	24
1.3.1 A rectification procedure . . . . .	24
1.3.2 A simplified rectification procedure . . . . .	25
<b>2 Calibration</b>	<b>27</b>
2.1 Calibration of the model's parameters . . . . .	27
2.1.1 Shocks . . . . .	28
2.1.2 Aircraft velocity . . . . .	29
2.1.3 Aircraft velocity variations . . . . .	29
2.1.4 Elementary time-step . . . . .	32
2.1.5 Performance . . . . .	32
2.2 Validation of the Model Assumptions . . . . .	33
2.2.1 Validation Meeting . . . . .	33
2.2.2 Expert's feedback . . . . .	34
2.2.3 Addressing expert's feedback . . . . .	35
<b>3 Input Data Generation</b>	<b>36</b>
3.1 Flight Plan Generator 1 module: from M1 real trajectories . . . . .	36
3.2 Flight Plan Generator 2 module: from M1 simulated trajectories . . . . .	37
3.3 Pre-tactical de-conflicting module . . . . .	39
<b>4 Results</b>	<b>40</b>
4.1 Results on a single ACC: capacity stress-test . . . . .	41
4.2 Results on different ACCs . . . . .	47
4.3 Results on Look-Ahead . . . . .	57
4.3.1 Velocity Noise . . . . .	57
4.3.2 Look-Ahead and Shocks . . . . .	58

4.3.3 M1 Capacities . . . . .	64
4.4 Results on the Multi-sector ABM . . . . .	67
4.5 Validation of results and identification of operational benefits . . . . .	73
FINAL REMARKS . . . . .	74
BIBLIOGRAPHY . . . . .	76

# List of Figures

1.1	Illustration of the time discretization used in the model. . . . .	15
1.2	Illustration of the procedure we use to optimize the procedure we use to check flight trajectories done against the other. . . . .	17
1.3	The figure illustrates the procedure of re-routing, see text for more details. The dashed trajectories, although possible, were not selected because the angles between the modified and planned trajectories were larger than $\alpha_M$ . $T_5$ was not considered because the segment $BT_5$ would cross the shocked area. . . . .	19
1.4	Illustration of the flight-level change sub-module. . . . .	20
1.5	The figure illustrates the procedure of issuing directs. . . . .	21
1.6	The figure illustrates the techniques of re-routing when the ACC is splitted in sectors, see text for more details. When the capacity of sector $S_2$ is exceeded, the module redirects the aircraft to the navigation point $E'$ rather than $E$ as in Fig. 1.3. . . . .	22
1.7	The figure illustrates the techniques of rectification that we use in order to generate surrogate M1 scenarios with increasing efficiency. . . . .	25
1.8	The figure illustrates the simplified technique of rectification that we use in order to generate surrogate M1 scenarios with increasing efficiency. . . . .	26
2.1	Velocity distribution measured from the M1 files. . . . .	29
2.2	Distribution of percentage difference of velocity (M3, M1). The two vertical red lines indicate the best $x_{min}$ for the two tails, selected by using the procedure sketched above. . . . .	30
2.3	Cumulative distribution of delay in the simulated and real data when the distribution of velocities in each trajectory segment is calibrated with velocities maintained by aircraft obtained from real M3 data. . . . .	31
2.4	Box-plot of delay in real data for different aircraft type. The shown error bars are the standard deviations. The boxes correspond to the first and third quantile. . . . .	31
2.5	Percentage of conflicts un-detected by the model for different values of $\delta t$ . The percentage is computed with reference to the number of conflicts detected with $\delta t = 1$ sec. The red line corresponds to a 1% loss of conflicts . . . . .	32
3.1	Empirical probability distribution of the number of flights between origin and destination airports (left panel) and empirical probability distribution of flight level occupancy in day 06/05/2010, LIRR ACC. . . . .	36
4.1	Simplified graphical representation of a simulation at a certain time. The green lines represent the M1 flight trajectories. The blue circles represent the aircraft active in the sector at that time instant in the central flight level. The magenta circles represent the aircraft active in the sector at that time instant in the lowest or highest flight level. The red spot represents a shocked area. . . . .	41

4.2	Distribution of time departure for the de-conflicted (blue line) and original M1 flight trajectories (green line). . . . .	42
4.3	Average number of conflicts detected in the surrogate M3 flight trajectories of the LIRR ACC, for different values of efficiency (horizontal axis) and for different values of the aircrafts present in the ACC (different lines in the plot). Each of the shown curves has been normalized with $N_f^2$ that represents the maximum possible number of conflicts in an environment with $N_f$ aircraft. . . . .	43
4.4	Average number of possible safety events (PSE) detected in the M1 flight trajectories of the LIRR ACC, for different values of efficiency (horizontal axis) and for different values of the aircrafts present in the ACC (different lines in the plot). Each of the shown curves has been normalized with $N_f^2$ that represents the maximum possible number of conflicts in an environment with $N_f$ aircraft. . . . .	44
4.5	comparison between the number of actions done by the controllers when we implement the Haversine distance (red) and the Euclidean distance in the LIRR ACC. These curves are obtained by considering 10 simulations in which 70% of aircraft is randomly delayed by a maximum of 5 min and the ABM is working in the current scenario. The time needed to perform one simulation with the Haversine distance is 10.7 sec, while considering the Euclidean distance we go down to 4.2 sec. . . . .	45
4.6	Scatter Plot of the average number of conflicts detected in the surrogate M3 flight trajectories versus the average number of possible safety events (PSE) of the LIRR ACC. Different points represent different values of efficiency and different values of the aircrafts present in the ACC. . . . .	46
4.7	Density map of the PSEs detected when considering three different values of efficiency and $T_{thresh} = 5.0$ min in the LIRR ACC. In the left panel we show the PSEs detected starting from the real M1 trajectories, i.e. of $E = 0.9729$ . In the right panel we show the PSEs detected starting from the M1 trajectories corresponding to the SESAR scenario, i.e. with an efficiency value of $E = 0.9999$ . In the central panel we show the PSEs detected starting from the M1 trajectories corresponding to the intermediate value of efficiency $E = 0.9800$ . To enhance readability, we first take the logarithm of the number of PSEs and then we normalize by dividing all logarithms by the maximum one. . . . .	47
4.8	Scatter-plot of the efficiencies of the M3 surrogate trajectories obtained after running the ABM versus the original efficiency measured for each of the 15 ACCs and in the two extreme cases of $p_d = 0$ (blue circles) and $p_d = 1$ (red circles). . . . .	49
4.9	Scatter-plot of the efficiencies of the M3 surrogate trajectories obtained after running the ABM versus the original efficiency for all the 39 target efficiencies of Table 4.2 and in the two extreme cases of $p_d = 0$ (blue circles) and $p_d = 1$ (red circles). The right panel is a zoom of the region around $E = 0.9999$ . . . . .	50
4.10	Number of re-routings (top panels) and number of flight level changes (central panels) and total number of actions (bottom panels) for each of the 15 ACCs and in the two extreme cases of $p_d = 0$ (right panels) and $p_d = 1$ (left panels). . . . .	51
4.11	Gain metric of Eq. 4.1 computed for each of the 15 ACCs and in the two extreme cases of $p_d = 0$ (bottom panel) and $p_d = 1$ (top panel). . . . .	52
4.12	Scatter-Plot of the number of flight level changes versus the number of re-routings. The blue points correspond to the 15 ACCs considered with their original efficiency values, i.e. the one corresponding to the scenario. The red points correspond to the 15 ACCs considered with their unitary efficiency values, i.e. the one corresponding to the SESAR scenario. The green points correspond to the intermediate values of efficiency reported in Table 4.2. . . . .	53

4.13 Number of re-routings as a function of the Number of Flights. The blue points correspond to the 15 ACCs considered with their original efficiency values, i.e. the one corresponding to the scenario. The red points correspond to the 15 ACCs considered with their unitary efficiency values, i.e. the one corresponding to the SESAR scenario. The green points correspond to the intermediate values of efficiency reported in Table 4.2. . . . .	54
4.14 Number of Flight level changes as a function of the Number of Flights. The blue points correspond to the 15 ACCs considered with their original efficiency values, i.e. the one corresponding to the scenario. The red points correspond to the 15 ACCs considered with their unitary efficiency values, i.e. the one corresponding to the SESAR scenario. The green points correspond to the intermediate values of efficiency reported in Table 4.2. . . . .	54
4.15 Distribution of the number of re-routings for a few selected values of efficiency in the case when we issue directs (right panel) and in the case when $p_d = 0$ (left panels). The red lines correspond to a reference gaussian distribution with mean and variance taken from observed data in the case when $p_d = 1$ and to a reference Poisson distribution with mean and variance taken from observed data when $p_d = 0$ . . . . .	55
4.16 Evolution of the number of actions of the controllers with the noise on velocity . . . . .	58
4.17 Number of actions of the controller for different number of shocks happening in the area. . . . .	59
4.18 Evolution of the number of changes of altitude (left) and number of reroutings (right) as a function of the look-ahead for different number of shocks in the current scenario (unrectified trajectories). . . . .	59
4.19 Spatial locations of the actions taken by the controller (only changes of altitude). Left panels: low number of shocks. Right panels: high number of shocks. Top: low look-ahead. Bottom: high look-ahead. The figures have been obtained with 10 tactical simulations for 2 strategic simulations. The number displayed are the sum of the actions taken in the 20 simulations. The contours have been smoothed out with cubic spline interpolation to facilitate the reading. . . . .	60
4.20 Heterogeneity of the changes of altitude as a function of the number of shocks (left) and the look-ahead (right). . . . .	61
4.21 Heterogeneity of the reroutings as a function of the number of shocks (left) and the look-ahead (right). . . . .	62
4.22 Evolution of the number of changes of altitude (left) and reroutings (right) as a function of the look-ahead and the number of shocks in the SESAR scenario (straight trajectories). . . . .	62
4.23 Spatial locations of the actions taken by the controller (only changes of altitude) in the SESAR scenario. Left panels: low number of shocks. Right panels: high number of shocks (400). Top: low look-ahead. Bottom: high look-ahead. The figures have been obtained with 10 tactical simulations for 1 strategic simulation. The number displayed are the sum of the actions taken in the 10 simulations. The contours have been smoothed out with cubic spline interpolation to facilitate the reading. . . . .	63
4.24 Heterogeneity of the changes of altitude as a function of the number of shocks (left) and the look-ahead (right) in the SESAR scenario. . . . .	64
4.25 Heterogeneity of the reroutings as a function of the number of shocks (left) and the look-ahead (right) in the SESAR scenario. . . . .	64

4.26	Different scaling for different scenarios. The scatter plots have been obtained with a uniform reduction of the capacities (light blue), with some sectors severely impaired (violet) and without any capacity (red). The solid lines are the result of linear power law regressions for each set of data. . . . .	65
4.27	Different scaling in different scenarios for the number of actions as a function of the number of flights in the area in the case of straight trajectories. In red, the simulations were done without capacities. If blue, constant capacities were applied. . . . .	66
4.28	Sectors in the italian LIRR ACC. . . . .	67
4.29	Efficiency of the surrogate M3 trajectories as a function of the sectors capacity. . . . .	68
4.30	Scatter-plot showing $\overline{EX}$ defined in Eq. 4.2 for the current (vertical axis) and SESAR scenario (horizontal axis). The values shown are averages performed over 1000 simulations. The color code indicates the 8 considered values for the average number of shocks per time-step per flight-level $S_m$ . . . . .	69
4.31	Sectors occupancy over the 24 hours for a specific value of the number of shocks $S_m = 1.071$ for the current and the SESAR scenario. When red is visible this indicates that occupancy in the M1 files is larger than in the M3 files. The opposite when yellow is visible. Orange indicates that occupancy in the planned trajectories equals capacity in the simulated trajectories. In the left panels we show the results relative to the current scenario, while in the right panels we show the results for the SESAR scenario. . . . .	71
4.32	Number of re-routings (blue line) and Number of flight-levels (green line) for the current (left panel) and SESAR (right panel) scenario as a function of the number of shocks $S_m$ . The error-bar of the first point in the central panels is very small as it was obtained for simulations without shocks and therefore quite stable. . . . .	72

## DISCLAIMER

The results shown in the present deliverable are preliminary and must be merely intended as indicative of the model's capabilities.

An extensive debugging procedure is ongoing and it will be part of the activities to be performed during the second part of the ELSA project extension relative to the release of a portable version of the model.

## INTRODUCTION

This document presents the work done for the development of the Agent Based Model during the extension of the ELSA project. The deliverable describes the different modules of the model and the way numerical simulations have been implemented. We also illustrate some of the results obtained with the model. Our intention is to show all the features of the model. For this reason we performed simulations with the aim of showing how the different modules of the model can work. Therefore, the results illustrated in section 4 must be intended as indicative of the model's capabilities. Some of the topics touched upon in section 4 will be further deepened in future research publications.

The document is divided in four main parts.

In chapter 1 we describe the model's objectives and its different modules that try to implement them. The model in its present form shares its main features with the tactical layer of the Agent Based Model already presented in deliverable D2.3 [1]. Presently the models works at the level of ACCs and we also have the possibility of implementing sectors with fixed capacity within the ACCs. Since one of the main aim of the model is to provide scenario simulations of the future SESAR scenario, we also implemented a module that allows to move in a controlled way from the current to the future SESAR scenario.

In chapter 2 we present the activities that we have conducted in order to calibrate some of the model's parameters and to validate the main assumptions of the model with the help of SESAR experts and ATC controllers. We also indicate how the feedback from the validation activities have been transferred to the model.

In chapter 3 we describe the ABM modules that provide the input data to the model. In fact, we have two modules: one that works on real M1 files and the second that works on fully surrogate data. The first flight plan generator does not take into account capacity constraints. The second module takes into account sectors capacities and it is essentially based on the strategic layer of the ABM presented in deliverable D2.3, thus realizing the objective of integrating the strategical and the tactical layer of the models presented in D2.3 [1].

Finally, in chapter 4 we illustrate the model capabilities by performing a few simulation experiments. We describe the results obtained with the simulation experiments:

- we perform capacity stress tests on a single ACC not partitioned into sectors. This should mimic the condition where the progressive integration of the airspace foreseen by SESAR has reached the full deployment.
- we perform a comparative analysis of different ACCs in order to show the heterogeneity of behaviors that can be revealed by the model.
- we perform a few numerical experiments by changing some model parameters, mainly the controller's look-ahead and the number of shocked areas during the day.
- we then move to perform experiments on a single ACC partitioned into sectors showing how the model behaves in presence or in absence of shocked areas.

## EXECUTIVE SUMMARY

This document presents the work done for the development of the Agent Based Model during the extension of the ELSA project. The deliverable describes the different modules of the model and the way numerical simulations have been implemented. We also illustrate some of the results obtained with the model. Our intention is to show all the features of the model. For this reason we performed simulations with the aim of showing how the different modules of the model can work. Therefore, the results illustrated in section 4 must be intended as indicative of the models capabilities. Some of the topics touched upon in section 4 will be further deepened in future research publications.

Chapter 1 is devoted to the description of the model, Chapter 2 illustrates the main activities performed for the calibration of some model parameter and the validation of the main model's assumptions. Chapter 3 describes the modules that are used to generate the data that feed the model. Chapter 4 is devoted to an illustration of some results obtained with the model. We performed simulations with the aim of showing how the different modules of the model can work. Therefore, the results illustrated in this section must be intended as indicative of the models capabilities.

One of the main results obtained in section 4.1 was that the number of actions performed by the controller rescales with  $N_f^2$ , where  $N_f$  is the number of aircraft present in the sector, see Fig. 4.3. Moreover, Fig. 4.6 indicates that given the number of possible conflicts as measured from the M1 files, the average number of actions that a controller has to perform in order to avoid conflicts can be predicted in terms of a linear law. Specifically, the figure shows the existence of two different linear regimes. For values of efficiency close to unity the curve can be fitted with a linear relationship whose slope is of the order of 0.05, while for lower values of efficiency we have a linear relationship whose slope is of the order of 0.01. Finally, Fig. 4.7 indicates that the number of possible conflicts in the SESAR scenario is predicted to be more spread all over the considered ACC, rather than concentrated in specific points as in the current scenario. This might explain why on average we expect a smaller number of actions to be performed by the controls in the SESAR scenario with respect to the current scenario, see again Fig. 4.1.

The investigations performed in section 4.2 on different ACCs confirm the expectation of a smaller number of actions to be performed by the controls in the SESAR scenario. However, we were not able to find any universal law able to describe the behavior of different ACCs in a unified way. This would then imply that the specific details of an ACC (geographic area, number of aircraft, structure of the current scenario navigation point network) play an important role. One possible common feature between the different ACCs is that the distribution of number of reroutings for the vast majority (35 out of 39) of the ACCs seems to follow a Gaussian distribution when the issuing of directs is allowed, while this no longer true when directs are not allowed. The importance of this issue lies in the fact that the gaussianity ensures that on average the probability that a controller performs a large number of actions remains low.

In section 4.3 we mainly investigate what is the role of having a larger look-ahead in the management of the conflicts. Fig. 4.22 shows that indeed enlarging the look-ahead brings a decrease in the number of the actions that the controller has to do. Moreover, after a certain time horizon of about

25 minutes the number of reroutings seems to be independent of the average number of shocked areas. It is also interesting to compare the spatial distribution of shocks when there is an high number of shocks and a low look-ahead (top-right panel of Fig. 4.23) and an high number of shocks and a large look-ahead (bottom-right panel of Fig. 4.23). The two mentioned panels indicate that indeed with a larger look-ahead the management of the trajectories improves drastically. Furthermore, a comparison between Fig. 4.19 and Fig. 4.23 indicates that in the SESAR scenario there is an overall better management of the trajectories with respect to the current scenario.

In section 4.4 we investigate the capabilities offered by the implementation of sectors within the ACC. In the present version of the model, although the existence of sectors inside the ACC is permitted, the air traffic management is uniform, meaning that we have controllers that manages the aircraft within the ACC with the same rules. This is done in view of the fact that at the level of ACC there is a certain uniformity of behavior amongst the controllers of different sectors, also due to the fact that they are all working in the same physical place. This also contributes to have a lower level of coordination amongst controller, with respect to the case of controllers working on sectors belonging to different ACCs. One of the main results of this section is that in the SESAR scenario the sectors' occupancy exceeds capacity in a smaller number of cases and for less time, as can be seen by comparing the results of Fig. 4.30 and Fig. 4.31.

# 1 Model

At the most elementary level, the airspace is divided in 3-D airspace volumes, termed *elementary sector*, or *collapsed sector* (called simply *sector* in the following). A sector is handled by two controllers: one (*executive*) is responsible of keeping the adequate separation between aircraft in the sector (making sure they do not infringe the separation minima), while the other one (*planner*) is responsible for the coordination with the adjacent sectors and the planning of the modified trajectories. The sectors are dynamic entities, which can be split or aggregated depending on the air traffic load. Moreover, the sectors can be roughly divided in two types: the en-route sectors, controlling the planes in their en-route trajectory, and the Terminal Maneuvering Areas (TMA) or the Control Zones (CTR), managing the take-off and landing phases. The first important level of aggregation of sectors is given by the ACC, where all the sectors are physically controlled from the same room (control center). The model is able to work on the whole 3-D volume of the airspace, while all results presented here are considering only the portion of airspace above FL 240.

The agents of our agent-based model are aircraft/pilots and air traffic controllers who are active within an *Area Control Center* (ACC) in the European airspace.

We model and simulate the events that make a planned flight trajectory, recorded in the so-called M1 files, transform into an actual one, recorded in the so-called M3 files. The aim is that of investigating the issues that affect the predictability<sup>1</sup> of the last filed flight-plan within the ATM system, and what are the changes brought by SESAR in terms of airspace management and controllers' workload. The specific scientific questions we are investigating are:

- What are the issues that affect the predictability of the last filed flight-plan within the ATM system? How is the predictability affected by these issues?
- Can sectors capacity be improved by a more efficient management of conflicts?
- What are the impacts of the changes foreseen by SESAR on the airspace management and on the controllers' workload?
- Are these changes able to accommodate efficiently the foreseen traffic increase?

## 1.1 General features of the model

The interaction between the agents considered in our ABM is needed in order to manage the tactical changes occurring in the system due to unforeseen events, i.e. weather events, congestions, limitation of sectors capacity, etc. Moreover, the ATC sectors are the places where flight trajectories are made conflict free.

The model takes into account that M1 trajectories are not conflict free. Thus one main task to be performed within the model is to deconflict trajectories. Moreover, we simulate shocks in the system

---

<sup>1</sup>Predictability is here intended as a comparison of the actual flight arrival time to the scheduled flight arrival time.

and see how the system reacts to them. We assume that the shock lasts for a certain time window. Operatively, this means that for a certain time window a certain area of the sector or ACC can not be crossed by flights. This might correspond to a situation where an extreme weather event occurs and therefore the air traffic must be deviated [2, 3]. As a result, another task of the model is to modify one or more flight trajectories in order to avoid these shocked areas. The way we model this step is to deviate the flight trajectories along new navigation points that are external to the restricted area and with the constraint that (i) we want to minimize the length of the deviated trajectory and (ii) the deviated trajectory must be conflict free. We will perform different simulation experiments by varying the number and extensions of shocks.

In general we will take into account three different critical situations: (i) there is the onset of a shocking area, (ii) there is a possible conflict of trajectories that nevertheless do not intersect one with each other and (iii) there is a possible conflict of trajectories that intersect with each other. The last two cases are essentially the same from an operative point of view. We keep this case distinct from the previous one to emphasize that the last case usually occurs mainly in the planned trajectories, while the previous one usually occurs mainly when one of the two conflicting trajectories have already been deviated. In any case the way our ABM treats these three different situations is the same. Starting from the planned trajectory, we identify the navigation point(s) involved in the critical situation and try to select new navigation point(s) for each flight trajectory such that the new trajectory has the minimal length and it is conflict free. This algorithm is therefore essentially based on “re-routing” and the possibility of performing flight level changes.

When a trajectory is deviated, then in general the aircraft is sent back to its planned trajectory. The algorithm we have implemented looks for a new trajectory that allows the aircraft to come back to its planned trajectory within the considered ACC. In general an aircraft in sector  $S_A$  when re-routed can be directly sent to another sector  $S_B$  if such choice is preferable in terms of trajectory length. However, if sending the aircraft to a new sector  $S_B$  would infringe the capacity of that sector, the algorithm searches for a sub-optimal modified trajectory trying to send the aircraft back to the planned trajectory within the same sector  $S_A$ .

Whenever possible, the model allows for the issuing of directs. They are given within the ACC in order to speed up the passage of the aircraft within the ACC, provided that no conflict is created.

We have constructed the code in a modular way that allows to swap the priority of the strategies adopted by the controllers. In fact, as a default controllers first check for the possibility of doing re-routings and then change the flight altitude. However, if necessary, we can easily modify the code in such a way that the two strategies mentioned above are swapped or that, if needed, no direct is issued.

For each simulated flight we will monitor two variables. First we will consider the number of actions that controllers performed for each flight. This will simply be the number of changes (re-routings, flight level, ...) operated on the planned trajectory. We also measure how the different trajectories are changed (no matter how many times) by comparing the length of the planned and the modified trajectory.

The modules described below implement a local resolution of conflicts. However, this way of solving conflicts (i) can be slow from a computational point of view and (ii) provides solutions that are not optimized at a global level, thus making it necessary to “adjust” trajectories several times as long as an aircraft travels across the ACC. We are fully aware of this limitation in our model. Indeed, we implemented such solution because we had indications that this is close to the way controllers work in reality. Moreover, we also believe that our solution might be quite effective in the SESAR scenario simulations. In fact, we might simulate a scenario where controllers have a role less preeminent than in the current scenario and some basic conflict-resolution actions are left to the single aircraft. In this respect, our model might mimic a scenario where pilots, that clearly have not a global vision of the system, endowed with a set of policy rules assigned by their airlines, will perform an *active*

conflict resolution at a tactical level, thus realizing a sort of self-organization amongst aircraft.

## 1.2 Implementation of the Model

The code that implements the model is written in C [4] and Python [5].

In the results presented in this deliverable, the model works at the level of a single ACC. Having that, in the current version of the model we consider shocked areas which are totally included in the ACC and that do not involve navigation points on the boundaries. The shocks may in principle be located in different ATC sectors within the ACC. However, the model can easily be adapted to work on a large airspace on interest eventually partitioned into smaller pieces.

Below we describe the different modules of our model.

### 1.2.1 Time-step choice

The ABM is of course a discrete-time model. Therefore the first thing to do is to introduce an efficient time discretization. In fact, we consider two typical times in the model: the time-step  $\Delta t$  and the elementary time-increment  $\delta t$ , see Fig. 1.1. While the elementary time-increment  $\delta t$  is the one that allows a finer sampling of the trajectories, the  $\Delta t$  time-step is the time horizon over which the controller knows the flight trajectories to be managed.

In fact, the model works by sampling the position of each aircraft at each time  $t_i$  where  $\delta t = t_{i+1} - t_i$  is typically of the order of 8 sec and there are  $N$  elementary time-increments within each time-step  $\Delta t$ . Therefore the time-step is of  $\Delta t = N\delta t$  seconds. The aircraft travels with constant velocity from one sampling point to the successive.

Additionally, we have implemented the fact that the model works on time-steps of length  $\Delta t$  that are overlapping with each other. Specifically, when the calculations are performed within a time interval  $[t, t + \Delta t]$ , the successive time interval is  $[t + t_r\Delta t, t + \Delta t + t_r\Delta t]$ , where the time-roll  $t_r$  is a number between 0 and 1, see blue vertical line in Fig. 1.1. By considering overlapping time-steps we avoid the effect of having a controller blinded at the end of each time-step. Its look-ahead will therefore be enhanced and in that way in worst case he will see a conflict  $(1 - t_r)N\delta t$  seconds in advance. In the time range  $[t, t + t_r\Delta t]$  the controller has a perfect knowledge of the flight trajectories. In the time range  $[t + t_r\Delta t, t + \Delta t]$  we assume that there is a degradation of the information and that, in particular, the controller has an imprecise knowledge of the aircraft velocity, see section 1.2.2.

At the successive time-step the ABM updates the starting position of each aircraft with the position observed at the time  $t_r\Delta t$ , see blue vertical line in Fig. 1.1.

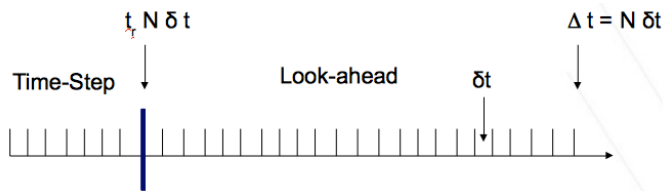


Figure 1.1: Illustration of the time discretization used in the model.

### 1.2.2 Velocity Noise Module

This module allows to introduce some errors in the forecast of the controller. Indeed, in the most simple setup, the controller is perfect in the sense that it forecasts exactly the right trajectories for

the flights within its time horizon. Hence, the only suboptimal decisions are taken because of the limited time-horizon. Section 4.3 is investigating this point.

In order to inject some errors on the positions of the flights, we introduce a parameter  $\sigma_v$ . Then for each flight we are doing the following:

- Between  $t = 0$  (current time) and  $t = t_r N\delta t$  (time of next update), we do not touch the forecast on positions. This is to ensure that there will be no actual conflict.
- Between  $t = t_r N\delta t$  and  $t = N\delta t$ , we change the velocity  $v \rightarrow v(1 + \delta v)$ , where  $\delta v$  is drawn at random from an uniform distribution in the range  $-\sigma_v$  and  $\sigma_v$ . Then the controller forecasts the position based on this new velocity.

The key point of this noise is the fact that the controller makes bigger errors on positions on longer horizon, and improves its forecast with time, until it is perfect below  $t_r \times \Delta t$ . Therefore,  $\sigma_v$  is not related to anything we might infer from data. Rather it is a proxy of how clever the controller is in performing reliable calculations in a short period of time to forecast the aircraft position.

We insist on the fact that the actual velocity do not change, and hence are always those of the planned trajectories (except, of course, in case of re-routing where the velocity is extrapolated on the new segment). In practice and without learning process, incorrect forecast or stochastic changes of the trajectories are indistinguishable.

Note that the shocks also introduce some errors in the forecast process, as we will also see again in section 4.3.

### 1.2.3 Navigation Points

Given the ACC, we populate it with navigation points. On one hand, part of the navigation points selected are real ones, i.e., those crossed by the flights according to their M1 last-filed flight-plan. On the other hand, other navigation points are generated randomly inside the ACC from an uniform distribution. These new navigation points could be seen as temporary points (!-points) in the M3 flight-plan. However, not all of them will be really used in the flights deviations. Only a set of them will be selected, as we will explain below. All the not used ones will be eliminated from the analysis after all the flights in the ACC will be checked. As we will explain in section 1.2.6.1, they are generated to allow the aircraft to deviate from the planned trajectories without necessarily passing over a predefined navigation point which might be too far.

### 1.2.4 Flight List module

Once the ACC has been populated with navigation points, we create a list  $FL_k$  of flights active in a specific time-step in the considered ACC. Such list will be reshuffled in the next time-step. This means that at each time step we randomly reorder the aircraft and therefore the order by which the aircraft are taken into account for conflict detection changes in each time-step. This is done in order to be sure that the trajectory to be deviated is not always the same one.

We have also the possibility of reordering this list according to a pre-specified rule or a scoring system. This option might be useful in the SESAR scenario as a way to implement different airline policies. For example, one might put in the higher part of the list those aircraft belonging to airlines prone to accept trajectory changes because in doing so they pay discounted fees to the air traffic providers. Analogously, one might put in the lower part of the list aircraft belonging to airlines less favorable to accept trajectory changes because they want to maximize predictability.

Within this list we check whether the flights are crossing a shocked area and whether or not they conflict with each other. Specifically, the  $i$ -th aircraft in the list will be checked against all other  $i - 1$  flights with  $j < i$ . However, not all the  $i - 1$  flights might have an interaction with  $i$ -th flight within

a certain time-step. In fact, if the distance between the starting position of the two  $i, j$  flights is larger than  $2 v_{max} N \delta t + d_{thr}$  it is impossible that the  $i$ -th and  $j$ -th flights will be involved in a safety event, see Fig. 1.2. Here  $d_{thr}$  is the typical distance threshold for safety events usually considered to be equal to 5 NM and  $v_{max}$  is the largest velocity of the aircraft active in the ACC. For this reason at each time-step the ABM first selects among the  $i - 1$  flights with  $j < i$  those who have possible conflicts according to the rule indicated above and then checks for conflicts only those in such subset. When a trajectory modification is needed, it will affect the  $i$ -th flight.

The reason for shuffling the list at each time step  $\Delta t$  is in order to avoid that the trajectory modifications are always applied to the same aircraft.

If a conflict involving the  $i - th$  is not solved by one of the strategies mentioned below, then the list is modified by putting the  $i - th$  in the first position in the list and trying to modify the other trajectories.

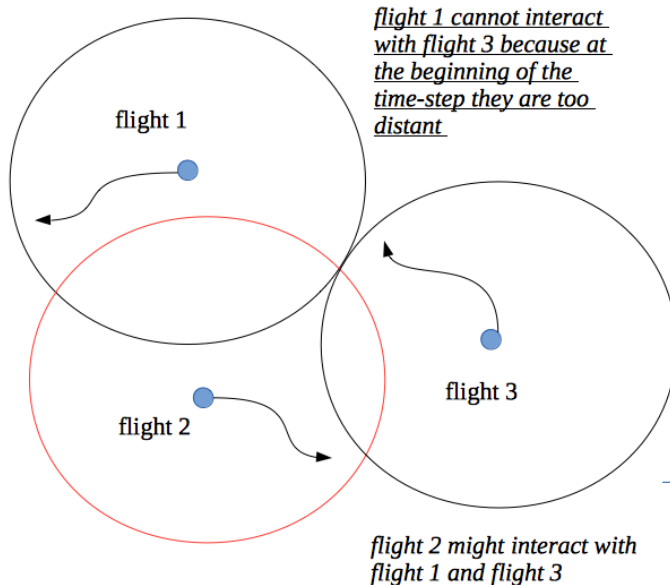


Figure 1.2: Illustration of the procedure we use to optimize the procedure we use to check flight trajectories done against the other.

### 1.2.5 Conflict Detection module

In order to check for collisions between two flights, we use a data structure that considers the aircraft localized inside the trajectory segments travelled within the given time-step  $\Delta t$ . For this purpose, as mentioned above, we introduce a finer subdivision of the time-step into  $N$  elementary time-increments  $\delta t$  and compute the real space-time position of the aircraft at each elementary time-increment, by assuming a constant velocity. The collision algorithm will have to simply calculate the positions of the aircraft for each of the elementary time-increments and then compute the distances between the two aircraft at these positions. Suppose we are now checking if the  $i$ -th flight trajectory is conflicting with all other  $f_j$  trajectories, with  $j < i$ , as mentioned above. We are therefore considering a maximal number of  $i - 1$  flight trajectories. For each of them we have an array  $\mathcal{P}_j$ ,  $j = 1, \dots, i - 1$  of length  $N$  given by the positions computed according to the algorithm illustrated above. For each of the  $N$  elementary time-increments, we compute an array of distances  $d^{(i)}$  of length  $i - 1$  choosing as a

value for each array element the minimum Haversine distance [6] between the  $i$ -th aircraft and all the other  $i - 1$  aircraft in the list with  $j < i$ . A possible conflict between two aircraft is detected whenever the elements of such an array are smaller than the safety distance threshold  $d_{thr}$  that is usually set to 5 NM. When a conflict is detected the algorithm proceeds to the next module that performs the de-conflicting of trajectories.

### 1.2.6 Conflict Resolution module

After the check for collision has been done, this module searches for a new conflict-free trajectory. It is conceived as a three-step algorithm that acts on the search of a new trajectory (re-routing) and the change of flight level, in case conflicts exist. The order by which these steps are applied might be changed.

The conflict resolution module is trajectory-based and performs a local resolution of conflicts by evaluating each pair of conflicting trajectories. The module works in 3-D as it takes into account the different flight levels at which aircraft are and issues flight level changes if needed.

#### 1.2.6.1 Re-routing submodule

The first step of the module we present here is the one that performs the re-routing. The procedure is illustrated in Fig. 1.3. We first identify the point  $B$  (not necessarily a navigation point) at which the aircraft is when the considered time-step begins. We then identify the navigation point  $A$  which is the first navigation point after the collision or the shocked area (filled circle in the figure). The idea is to (i) keep  $B$ , (ii) substitute  $A$  with a temporary navigation point and (iii) in case of conflicts eliminate all the navigation points between  $B$  and  $A$  of the planned trajectory within the considered time-step  $\Delta t$  and in case of shocked areas eliminate all subsequent navigation points inside the shocked area. Let us call  $E$  the first navigation point in the planned trajectory that we can keep.

To solve the conflict, we take the previously generated temporary navigation points  $T_k$  (squares in the figure) falling in a circle of radius  $D_{max}$  centered in  $B$ . We order them with respect to the angle that the segment connecting  $B$  and  $T_k$  forms with the original trajectory. We select the temporary navigation points that have an angle smaller than a certain critical value  $\alpha_M$ , see Table 1.1. We define as a new trajectory the one given by the two segments between  $B$  and  $T_k$  and between  $T_k$  and  $E$ . Amongst all the admissible  $T_k$  navigation points we select the one for which (i) the deviated trajectory has the smallest length and (ii) the angle between the planned trajectory and the segment between  $T_k$  and  $E$  is smaller than  $\alpha_M$ .

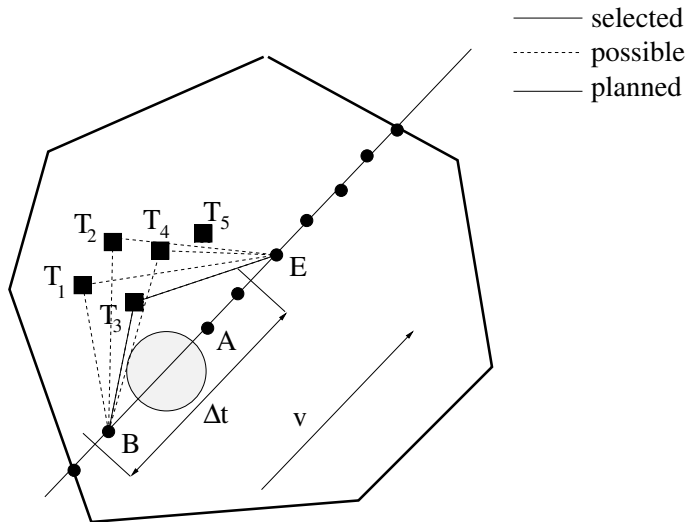


Figure 1.3: The figure illustrates the procedure of re-routing, see text for more details. The dashed trajectories, although possible, were not selected because the angles between the modified and planned trajectories were larger than  $\alpha_M$ .  $T_5$  was not considered because the segment  $BT_5$  would cross the shocked area.

If we do not find any temporary navigation point fulfilling these requirements we substitute E with the successive navigation point until the temporal distance between A and E is smaller than  $T_{max}$ . If no solution is found then the algorithm exits this sub-module and go to the next one.

When a trajectory is deviated, then in general the aircraft is sent back to its planned trajectory. The algorithm we have implemented looks for a new trajectory that allows the aircraft to come back to its planned trajectory within the considered ACC. In general an aircraft in an sector  $S_A$  when re-routed can be directly sent to another sector  $S_B$  if such choice is preferable in terms of trajectory length. However, if sending the aircraft to another sector  $S_B$  would infringe the capacity of that sector, the algorithm searches for a sub-optimal modified trajectory trying to send the aircraft back to the planned trajectory within the same sector  $S_A$ .

#### 1.2.6.2 Flight level change submodule

The second step of this module involves changes of flight level. A Flight level (FL) is defined as altitude above sea-level in 100 feet units measured according to a standard atmosphere but allowed flight levels are separated by 1000 feet, thus in principle 10 flight levels. However, according to the standard practice, in the following, a change of one FL is to be intended as a variation of 1000 feet in altitude (one separation level). Moreover, the semicircular rule has been considered, meaning that aircraft flying in opposite directions are allowed to fly only to odd or even FL respectively. Therefore when an aircraft needs to be moved to another FL, it will not be moved to the next first one but to the second one to respect the semicircular rule.

All flights are initially considered to be active in the planned M1 flight level. Therefore they can move two Flight Levels (FL) upwards or downwards whenever the re-routing is not feasible. The choice of the new level is done by considering the one where there is a smaller number of potential conflicts. If no level is available then the list is reshuffled by moving the considered flight in the first position.

As in the previous case, the flight is sent back to its trajectory within a time  $T_{max}$ .

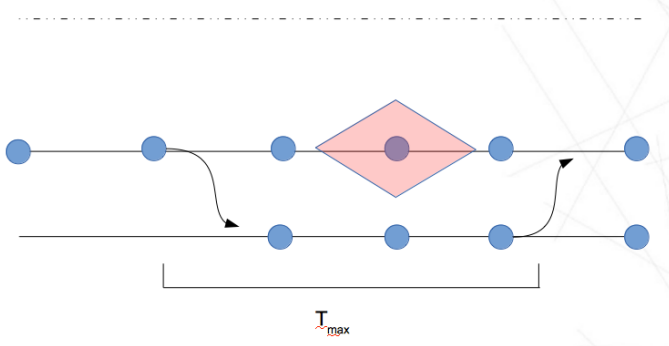


Figure 1.4: Illustration of the flight-level change sub-module.

#### 1.2.6.3 Velocity change submodule

The third step for changing the flight velocity is mainly based on a genetic algorithm that uses a mix of cross-over and mutation operators [7]. This module is written in C language in order to make it computationally efficient. In the data structure we are using in the present implementation of the model, we consider a unique value of aircraft velocity  $v$  for any elementary trajectory segment between two navigation points.

Suppose we are now checking if the  $i$ -th flight trajectory is conflicting with all other  $f_j$  trajectories, with  $j < i$ . We are therefore considering a number  $i - 1$  of flight trajectories. For each of them we have an array  $\mathcal{P}_j$ ,  $j = 1, \dots, i - 1$  of positions computed as illustrated above. When the Conflict Detection module identifies a subset of points within the  $j$ -th array  $\mathcal{P}_j$  such that these points are below the safety distance threshold, the ABM tries to solve the collision using a new module that implements a genetic evolutive algorithm. Assuming that the aircraft will run into  $N_{nvp}$  navigation points, the aircraft will therefore change  $N_{nvp} - 1$  velocities during its trajectory. In this step we first generate a population  $N_{pop}$  of velocities arrays each of length  $N_{nvp} - 1$ . We generate velocity arrays  $\mathcal{V}_s$ ,  $s = 1, \dots, N_{pop}$  filled with  $v_s$  velocities randomly selected under the condition that  $v_{min} < v_s < v_{max}$ , where  $v_{min}$  and  $v_{max}$  are the minimal and maximal velocity acceptable for the considered aircraft flying in the considered airspace. For each element of this population we compute the array of positions  $\mathcal{P}_s$ ,  $s = 1, \dots, N_{pop}$  with dimension  $N$ . For each  $\mathcal{P}_s$ ,  $s = 1, \dots, N_{pop}$  the algorithm computes the new trajectory length that can be used as a "fitness" value, according to the procedure illustrated in the re-routing module, see Fig. 1.3. The population of possible solutions (velocities arrays) will be sorted according to this fitness value.

The genetic algorithm searches for the optimal solution by applying to the population of velocities three different operators. Each one has a characteristic probability to be applied. Moreover, in order to avoid the selection of elements of the population that are too similar with each other, these operators will not be applied to the best element, but according to a probability function (a Gaussian distribution defined on the positive real axis, peaked in zero and normalized to unity in the interval from 0 to  $N_{pop}$ ). Each new element generated with these operators will take the place of the worst element in the population. These operators are applied on a random basis with different probabilities as to ensure that local minima are avoided.

#### 1.2.7 Directs module

If any conflict is detected, the ABM tries, with a probability  $p_d$ , to give a direct to the  $i$ -th flight, see Table 1.1. A direct is made by removing one or more navigation points of the M1 flight-plan after

the first navigation point present in the current time-step.

The algorithm first evaluates how many navigation points can be removed with the constraint that the flight has to come back on the original route within a time interval equal to  $T = 2 \Delta t$ , without infringing the sectors' capacities. Such choice of  $T$  has been done in agreement with the indications of the air traffic controllers consulted within the ELSA project. After that the model evaluates if the new route will be involved in conflicts (with other flights or shocks). If the direct is safe the new route is accepted, otherwise no direct is issued.

Finally, we have implemented a sensitivity threshold  $L_s$ . If the absolute difference between the length of the planned trajectory and the trajectory modified with the introduction of the direct is smaller than  $L_s$ , then we do not consider such direct. The threshold is set to  $L_s = 1$  km. This is done in order to avoid a proliferation of directs that have negligible impact on the improvement of the system efficiency.

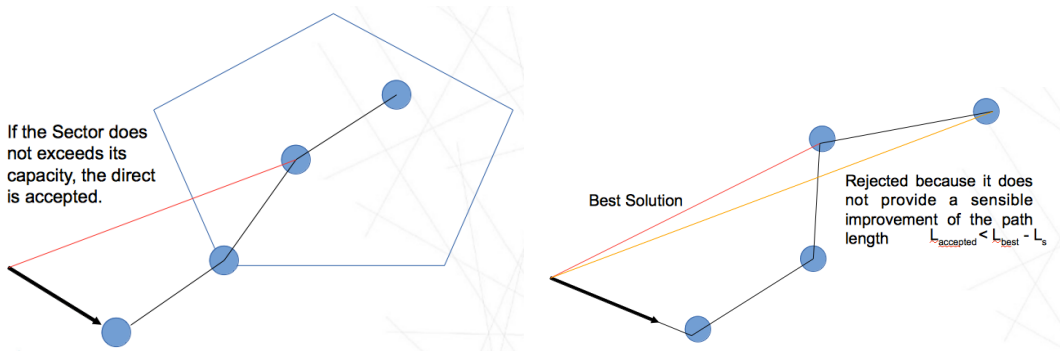


Figure 1.5: The figure illustrates the procedure of issuing directs.

### 1.2.8 Shocks module

In the current version of the ABM the shocks are modeled as circles of center  $C_S$  and fixed radius  $R_S$  and located at a flight level drawn from a random uniform distribution in the range  $[FL_{min}, FL_{max}]$ . Each shock vertically extends over 1 separation level, i.e. 1000 feet. Each shock has a duration drawn from a random uniform distribution in the range  $[1, D_S N \delta t t_r]$ . The area within these circles is inaccessible for the aircraft, and if a shock appears along an aircraft flight trajectory, the aircraft has to be re-routed or change flight level because all maneuvers are interdicted inside the shocks. We implemented the fact that there is an average number  $S_m$  of shocks per time-step per flight-level. In our model, the number of shocks will follow a Poisson distribution with mean  $S_m$ .

The position of the shocks is drawn from a list of points provided by the user. In this way the user can obtain a uniform distribution of the shocks inside the ACC providing a uniform distribution of the points  $C_S$ , or he/she can obtain different spatial distributions by providing an appropriate list.

At the beginning of each time-step the controllers cannot forecast the shocks. This means that they look at the current position of the shocks and they operate assuming that the shocks are fixed along the time-step  $\Delta t$  even if they could disappear within the  $t_r \Delta t$  time horizon. We can illustrate this issue with an example. Suppose we are considering an aircraft  $i$  at the time-step  $R_1 = [t, t + \Delta t]$ . As mentioned above, let us first consider the time interval  $R_{1,exact} = [t, t + t_r \Delta t]$ . This is the time range where the aircraft positions is known exactly. The controller has to decide what to do with the aircraft trajectory in the time range  $R_{1,l-a} = [t + t_r \Delta t, t + \Delta t]$ , which corresponds to the controller's look-ahead. Since shocks are issued every  $\Delta t$  seconds, all shocks occurring in the time

range  $R_{1,l-a}$  will be known by the controller not in the time-step  $R_1$ , but in the successive one  $R_2 = [t + t_r \Delta t, t + t_r \Delta t + \Delta t]$ . Therefore in the time-step  $R_1$  the controller manages the trajectory by assuming that even in  $R_{1,l-a}$  there are no shocks.

### 1.2.9 Multi-Sector module

The ACC we are considering is divided into a number of sectors. Each sector is characterized by its geographical extension and by its capacity, here intended as the maximum number of aircraft that can be contemporarily present in the sector within a certain time window.

The way we implement capacity in the sectors is by assigning a flag to each navigation point of the M1 files present in the sector. The flag indicates the sector a navigation point belongs to. We assume that the number of flights that can travel over each navigation point in a certain time-window is given by the sector's capacity. All navigation points on the boundaries between sectors have associated a zero flag. This value identifies the fact that no capacity constraint is assumed to exist on the sectors boundaries.

At each time-step the ABM evaluates the occupancy of each sector of the ACC. The occupancy is defined as the number of flights that will cross the sector within an hour.

When the occupancy of sector exceeds its capacity all the re-routings or directs that come from other sectors are rejected. Operatively this means that in a condition when occupancy equals or exceeds capacity any other incoming flight has to enter the sector from the M1 planned navigation points, see Fig. 1.6.

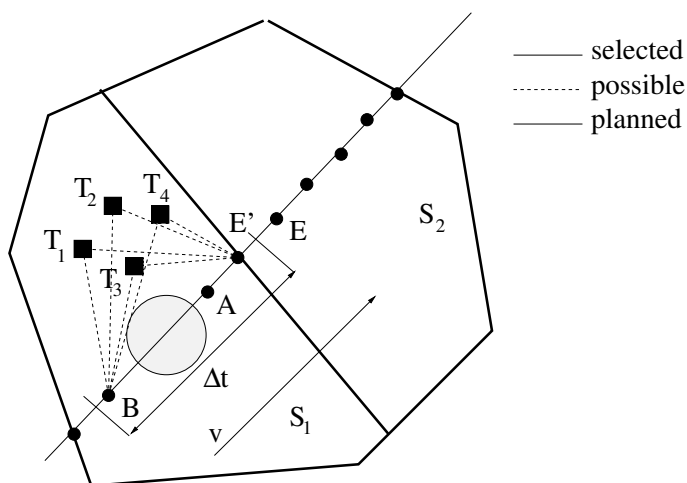


Figure 1.6: The figure illustrates the techniques of re-routing when the ACC is splitted in sectors, see text for more details. When the capacity of sector  $S_2$  is exceeded, the module redirects the aircraft to the navigation point  $E'$  rather than  $E$  as in Fig. 1.3.

In the present version of the model, the controllers behave in the same way, i.e. the models parameters summarized in Table 1.1 are the same for controllers in the different sectors. This is done in view of the fact that at the level of ACC there is a certain uniformity of behavior amongst the controllers of different sectors, also due to the fact that they are all working in the same physical place. This also contributes to have a lower level of coordination amongst controller, with respect to the case of controllers working on sectors belonging to different ACCs. Of course, when the model is used at the level of the ECAC airspace, one should implement that controllers might have different

behaviors and therefore the model's parameters should be selected in a different way for different controllers.

### 1.2.10 Model's parameters

In this section we summarize the model's parameters entering the different modules described above. In the third column we give a short description of the parameters and in the fourth column we introduce a categorization of the parameters in terms of the three categories described below:

- FP - free parameter, to be chosen according to the type of experiments one wants to perform.
- CD - parameter that needs to be calibrated from data.
- CV - parameter that needs to be calibrated according to the validation activities performed with ATM experts and ATCOs.

The parameters that need to be calibrated from data are really a few. However, there are many parameters (CV category) that are related to the behavior of controllers. In principle, these are parameters that could be inferred from data through some sophisticated data mining. However, we believe that these are the typical parameters that should be selected by consulting the ATM experts and ATCOs. On the other hand these are the parameters that one should change at will when performing scenario simulations to test how changing a certain feature will affect the ATM system.

ID	Parameter	Description	Type
1	$\Delta t$	Length of the time-step. This is also related to the controller's look-ahead.	FP
2	$\delta t$	Length of the elementary time-intervals.	FP
3	$t_r$	Fraction of $\Delta t$ by which we move the overlapping time-steps.	FP
4	$v$	aircraft velocity	CD
5	$\sigma_v$	Range of the noise introduced in the estimation of the aircraft velocity	CV
6	$D_{max}$	Radius of the circle centered in B where we look for temporary navigation points potentially relevant for performing a re-routing.	FP
7	$\alpha_M$	Maximum angle of deviation between planned and modified trajectory.	CV
8	$T_{max}$	Maximal temporal distance between the navigation point B and navigation point E that identify when a deviated portion of flight trajectory starts and ends.	FP/CV
9	$p_d$	Probability to try to issue a direct.	CD/CV
10	$L_s$	Sensitivity threshold for issuing a direct.	FP/CV
11	$v_{min}, v_{max}$	minimum/maximum velocity of aircraft present in the ACC	CD
12	$C_S$	Center of each shock.	FP/CD
13	$S_m$	Average number of shocks per time-step per flight-level.	FP/CD
14	$D_S$	Temporal duration of each shock.	FP/CD
15	$R_S$	Radius of each shock.	FP/CD
16	$FL_{min}, FL_{max}$	Minimum/maximum flight level where shocks are generated.	FP/CD

Table 1.1: Model parameters.

## 1.3 SESAR scenario trajectories

The model described above will be used to perform scenario simulations in order to investigate how predictability and capacity issues will change from the current to the SESAR scenario. To this end, we decided to model the SESAR scenario as the end-point of a spectrum of possible scenarios continuously ranging from the current to the SESAR scenario.

First of all we define a new metric called efficiency  $E$  in order to measure how different a given network of routes is with respect to the situation where any pair of airports (Origin and Destination) is directly connected by straight route. We define such efficiency as:

$$E = \frac{\sum_{N_f} d(O, D)_i}{\sum_{N_f} d_{BP}(O, D)} \quad (1.1)$$

where  $d(O, D)$  is shortest distance between Origin and Destination, while  $d_{BP}(O, D)$  is the Best Path distance on the route network identified by the navigation points. The sum is over all planned flights recorded in the M1 files. In this way the more a route is congested, the more weight it has. Another possible way to have an unweighted efficiency is to extend the sum above all possible routes. This metric takes values in the range (0,1]. Of course, the value  $E=1$  corresponds to the SESAR scenario.

### 1.3.1 A rectification procedure

We will move in a controllable way from the current scenario to the SESAR scenario by generating surrogate route networks each identified by a certain value of efficiency. This will be done by introducing a *rectification* of the current trajectories. This will allow us to study the transition between the current scenario and the SESAR scenario in a controlled way.

The algorithm requires as input a generic M1 file, i.e. a set of real planned trajectories, and produces as output another surrogate M1 with a larger target value of efficiency. At each step the algorithm evaluates the current efficiency and if it is less than the target efficiency performs the following steps:

- for any flight trajectory, the first and last point will not be modified, as they correspond to the origin  $O$  and destination  $D$  airports, see Fig. 1.7.
- then we randomly selects a navigation point  $P_i$  of a certain trajectory flight between the 2<sup>nd</sup> navigation point and the one before the last navigation point.
- we substitute  $P_i$  with the medium point  $M_i$  between the previous navigation point  $P_{i-1}$  and the next one  $P_{i+1}$ , see Fig. 1.7. In some case,  $P_{i-1}$  might coincide with the origin  $O$  or  $P_{i+1}$  might coincide with the origin  $D$ . This is not a problem given the fact that  $P_{i-1}$  and  $P_{i+1}$  are merely used as a reference.
- this procedure is iterated until the target efficiency is reached or all navigation points of all trajectories in the M1 files are modified.

At each iteration of the above steps the procedure maintains the number of navigation points present in the M1 files.

By using such procedure we can generate a set of M1 scenarios with increasing efficiency from the current scenario to the SESAR scenario characterized by unitary efficiency. We will therefore use the model described in the previous section to generate the corresponding sets of M3 files. We will be therefore able to investigate the modifications occurring from the current to the SESAR scenario in a controlled way.

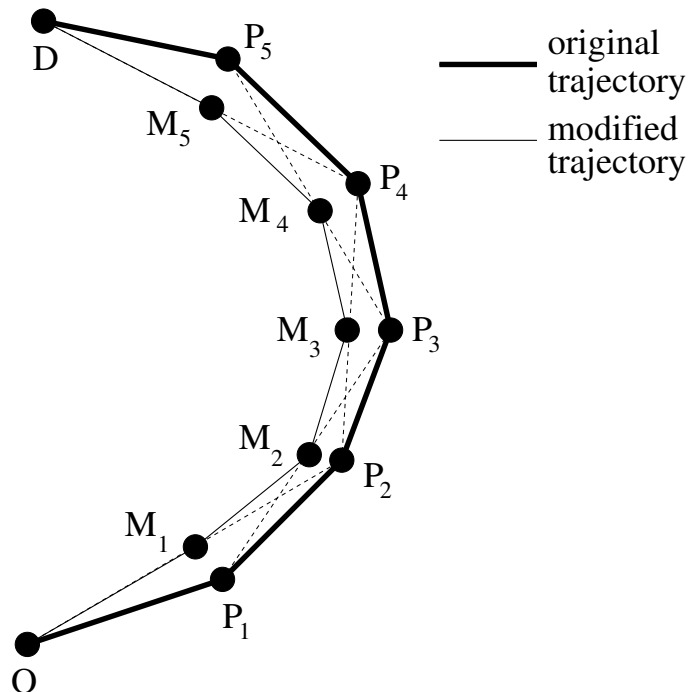


Figure 1.7: The figure illustrates the techniques of rectification that we use in order to generate surrogate M1 scenarios with increasing efficiency.

### 1.3.2 A simplified rectification procedure

The rectification procedure described above may be rather time consuming from a computational point of view. We have therefore devised a simplified procedure that reveals to be less time consuming and therefore more appropriate when we will have to perform several sets of simulations.

The alternative rectification is done in the following way. In a first step, a point  $P_i$  is chosen at random on a trajectory, like previously. However, the point is simply removed from the trajectory instead of being moved, i.e. the flight goes from  $P_{i-1}$  to  $P_{i+1}$  directly. The procedure goes on until the target efficiency is met.

In a second time, we resample the trajectories by generating new points on the trajectory so as to ensure that the agent-based model works properly. We do this by keeping the same number of navpoints between the remaining points on the trajectories that there were originally. Hence, the number of navigation points per trajectory is kept constant too. Figure 1.8 illustrates the procedure.

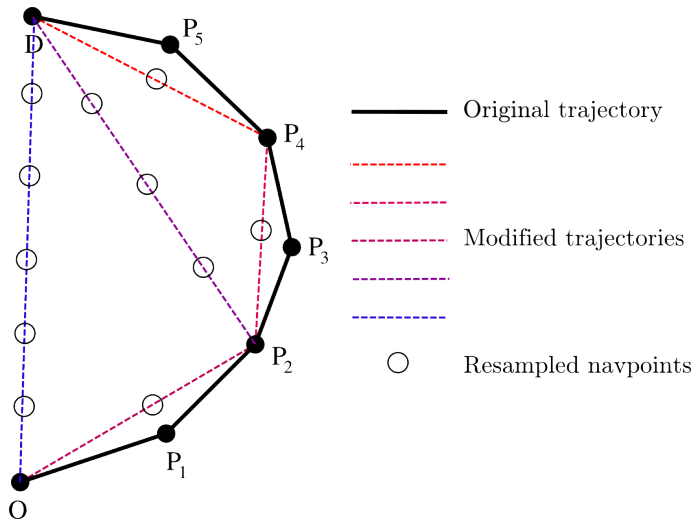


Figure 1.8: The figure illustrates the simplified technique of rectification that we use in order to generate surrogate M1 scenarios with increasing efficiency.

By summarizing, our model will give us the possibility of performing simulations of the current and SESAR scenario each of them characterized by:

- **current scenario:** low efficiency, no conflict-free trajectories, look-ahead of about 20 min
- **SESTAR scenario:** unitary efficiency, conflict-free trajectories, look-ahead up to 60 min

In both cases we can consider the possibility of giving or not directs ( $p_d = 0$  or  $p_d = 1$ ) and the possibility of having or not having sectors.

## 2 Calibration

### 2.1 Calibration of the model's parameters

As indicated in section 1.2.10, the parameters that for sure we have to calibrate from real data are

- the aircraft velocity  $v$ .
- the minimum/maximum velocity of the aircraft present in the airspace  $v_{min}$  and  $v_{max}$ .
- the probability by which directs are issued  $p_d$ .

Our choices for  $v$ ,  $v_{min}$  and  $v_{max}$  will be given in section 2.1.2. As for  $p_d$  we did not perform any calibration activity. In fact, we set  $p_d = 1$  (or  $p_d = 0$ ) because our idea was to show the potential of the model in an extreme case such as the one when trajectories are rectified whenever possible, i.e. a case when the planned flight trajectories are heavily modified ( $p_d = 1$ ) and when trajectories are not modified ( $p_d = 0$ ).

The input for the calibration activities of our model has been given by all flights of the LIRR ACC in day 6 May 2010, fulfilling the following constraints: (i) each navigation point of the route inside the sector is higher than at least 240 FL and (ii) the trajectory of the aircraft intersects the sector in two distinct points. The number of the flight trajectories fulfilling such constraints is:  $N=452$  for day 06 May 2010. However, the calibration has been done on the smaller subset of  $N_a = 380$  aircraft fulfilling the following further prescriptions: 1) flights are performed with Landplanes (i.e. no helicopter, gyrocopter, only aircraft which can only operate from or alight on land), 2) flights are scheduled, 3) flights have a IATA code 4) flights have a duration longer than 10 minutes. Further details on these filters can be found in deliverable D1.3 [8].

Other parameters have a mixed nature. In fact, the parameters relevant for setting the shocked areas:

- the center of the shocked area  $C_S$ .
- the radius of the shocked area  $R_S$ .
- the duration of the shocked area  $D_S$ .
- the average number of shocks per time-step per flight-level  $S_m$ .
- the flight level boundaries of the shocks  $FL_{min}$  and  $FL_{max}$ .

can either be calibrated from real data or considered as free parameters when performing scenario simulations. In fact, within the ELSA project we had not access to data about weather events. Therefore we decided to consider the above parameters as free ones, see section 4.4, taking into account the information reported in section 2.1.1 below.

We have then a set of parameters more related to the behavior of single controllers:

- the range for the velocity noise  $\sigma_v$ .
- the maximum angle of deviation from the planned trajectory when re-routing occurs  $\alpha_M$ .
- the maximum time after which aircraft come back to the planned trajectory  $T_{max}$ .
- the sensitivity threshold for issuing a direct  $L_S$ .

These are parameters which could in principle also be inferred from real data. However, we prefer to treat them as an input to the model in order to investigate whether with the considered input we obtain other empirical regularities observed in real data. Therefore, some of the calibration activities were conducted by directly interviewing an operational expert working in the Rome ACC. The interview regarded the features of such ACC and most of the operative knowledge acquired has been integrated into the model. The values of  $\alpha_M$ ,  $T_{max}$  and  $L_S$  indicated in Table 2.1 are part of the outcomes of such an activity.

The last set of parameters we have to consider in the model is given in the following list:

- the length of the elementary time-intervals  $\delta t$ .
- the length of the time-step  $\Delta t$ .
- the time roll parameter  $t_r$ .
- the radius relevant for conflict resolution  $D_{max}$ .

The values we have considered are reported in Table 2.1. The choice for  $\delta t$  is justified in section 2.1.4.

ID	Parameter	Description	Type
1	$\Delta t$	In section 4.1 and 4.2 $\Delta t = 20$ min. In section 4.3 we changed this parameter up to 60 min	FP
2	$\delta t$	8 seconds	FP
3	$t_r$	0.5	FP
5	$\sigma_v$	In section 4.1 and 4.2 $\sigma_v = 0$ . In section 4.3 we swept this parameter	CV
6	$D_{max}$	100 km	FP
7	$\alpha_M$	0.275 rad, i.e. $\approx 16^\circ$	CV
8	$T_{max}$	$2 \Delta t$	FP/CV
10	$L_S$	1 km	FP/CV

Table 2.1: Model's parameters choice.

### 2.1.1 Shocks

Part of the interviews with the operational experts regarded the general features of the shocks.

Adverse weather conditions occur on a daily basis and have a not negligible effect inside the ACC sectors and the system in general. This kind of events does not represent a challenge for the controllers that are always supposed to be capable of handling them. We have been able to identify two major classes of perturbations depending on their dimension:

- Small shocks ( $\approx 5$  NM of radius), with a fast dynamics and a short lifetime ( $\approx 1$  h), usually occurring during summertime.

- Large shocks (around  $60 \text{ NM} \times 20 \text{ NM}$ ), which can be considered static and with a lifetime that goes from 8 h to 10 h. This kind of perturbations represents big storms occurring during winter.

While the only possible way to manage a small shock is to avoid it, it is possible that the biggest one could be crossed by an aircraft instead of being avoided and thus generating a small delay instead of a large one. In fact, there might be big shocks composed by a set of smaller shocks localized in a certain geographical area, as to simulate a sort of porous medium where aircraft can pass through. In deliverable D2.3 [1] such issue was investigated by performing numerical simulations where the shocks were selected according to a gaussian distribution.

### 2.1.2 Aircraft velocity

The main calibration activity conducted on real data regarded the choice of the aircraft velocity.

In Fig. 2.1 we show the distribution of the aircraft velocity measure starting from the M1 files and in the LIRR ACC. The median of the distribution is  $v = 230 \text{ m/s}$  which correspond to  $v = 828 \text{ km/h}$ . This is the value that we used in the simulations of section 4.1 and section 4.2. From this distribution one might estimate  $v_{min} \approx 130 \text{ m/s}$  and  $v_{max} \approx 320 \text{ m/s}$ . The standard deviation is about  $\approx 22 \text{ m/s}$ .

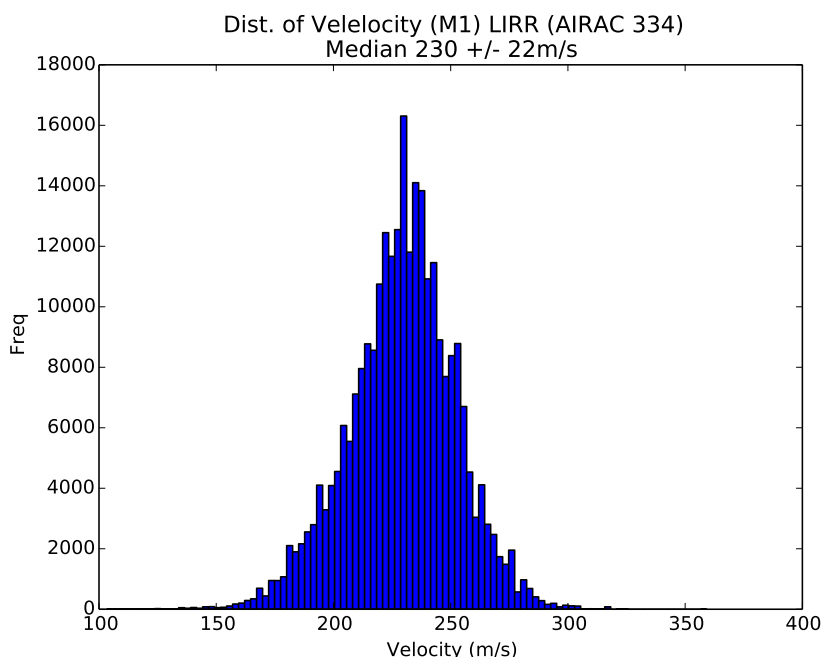


Figure 2.1: Velocity distribution measured from the M1 files.

### 2.1.3 Aircraft velocity variations

Another point we addressed during the calibration procedure is that the analysis of real data (AIRAC 334 - Sector LIRROV) shows a relevant difference between the planned velocity of aircraft and the actual one.

In order to investigate this aspect, we consider all trajectory segments<sup>1</sup> inside the sector LIRROV and calculate the percentage difference of velocity between M3 and M1 trajectories, i.e.  $v_r = \frac{V_{M3} - V_{M1}}{V_{M1}}$ . As shown in Fig. (2.2), the distribution of  $v_r$  shows exponential tails. This has been estimated by using the Kolmogorov-Smirnov test. In fact, we compute the K-S statistics for all subsets  $S_x = \{x_i : x_i > x_{min}\}$  obtained by considering different values of  $x_{min}$ . We then choose the first value of  $x_{min}$  with a p-value larger than 0.01, where the p-value was obtained by adapting the methodology illustrated in Ref. [9]<sup>2</sup>.

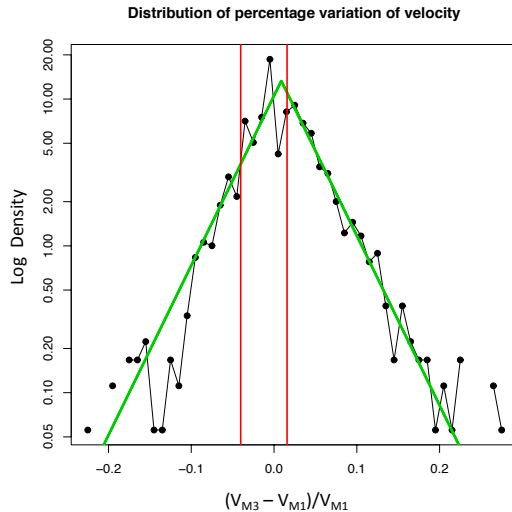


Figure 2.2: Distribution of percentage difference of velocity (M3, M1). The two vertical red lines indicate the best  $x_{min}$  for the two tails, selected by using the procedure sketched above.

We therefore decided to include in the ABM such an inaccuracy on the estimated velocity. Actually, for each aircraft, we modify the planned velocity in each segment according to a laplacian distribution with the same parameters observed in the real one. As a result the distribution of delays shows a good agreement with real data, as shown in Fig. 2.3. Also in this case we performed the K-S test obtaining  $K-S=0.0422$  and p-value  $p=0.4131$ . It is worth noticing that the main differences between model and real data are in the left tail of the distribution.

We investigated the relation between incorrect estimation and aircraft models. In fact, for the whole AIRAC 334, we computed the delay acquired in LIRROV by all aircraft fulfilling the STRONG filter introduced in Deliverable D1.1. We partitioned all these flights into 46 categories, according to the type of aircraft used in the specific flight. We calculated the distribution of delay for each of 46 partitions of different aircraft models. In Fig. 2.4 we show the average and standard deviation of these delays.

For each of the 1035 possible pair of aircraft type we calculated the Kolmogorov-Smirnov test, and only 36 pair of aircraft type resulted to have the same distribution of delay ( $p-value > 0.01$   $K-S < 0.1$ ). Therefore in general different aircraft types have different delay distributions. To compare

<sup>1</sup>Pairs of navigation points of the routes  $navigationpoint_i - navigationpoint_{i+1}$

<sup>2</sup><http://cran.r-project.org/web/packages/poweRlaw/vignettes/poweRlaw.pdf>

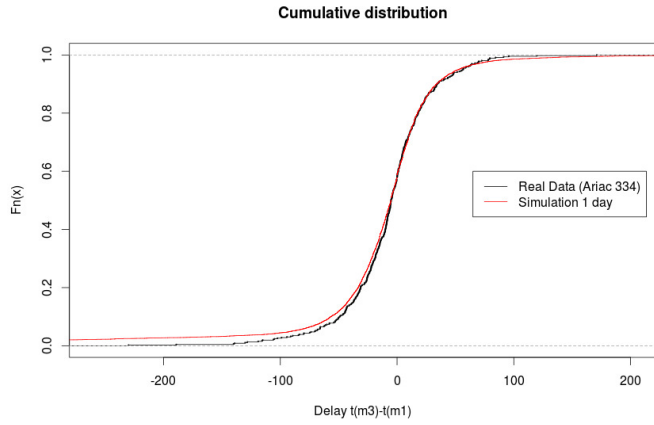
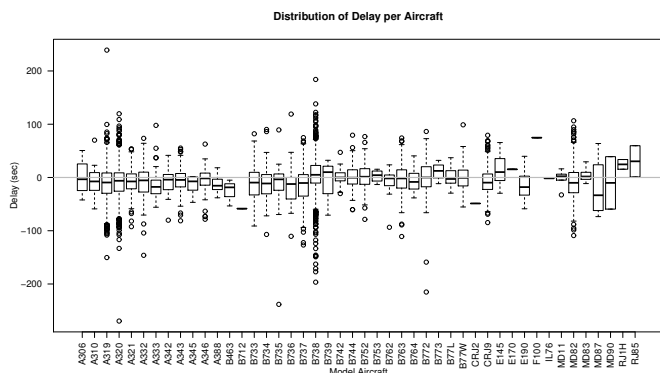


Figure 2.3: Cumulative distribution of delay in the simulated and real data when the distribution of velocities in each trajectory segment is calibrated with velocities maintained by aircraft obtained from real M3 data.

this value with a random null hypothesis we performed a bootstrap (without repetitions) taking into account that we have an heterogeneous system in term of partition size, i.e. the number of flights with a certain aircraft type. This was made by a random resampling of the partitions preserving the same size and extracting value from the entire sample. We performed 3000 bootstrap replica and for each one we calculated the number of distribution that K-S test recognize as identical. From this analysis we obtained 103 average number of pairs with identical distribution, with standard deviation 13.5. We checked that the observed value of 36 pairs observed in real data is statistically significant at a 1% significance threshold. We can thus conclude that there is a relation between aircraft model and incorrect estimation of velocity.



### 2.1.4 Elementary time-step

As mentioned above the choice of  $\delta t$  is something that can not be done by looking at data. In most of the simulations we considered  $\delta t = 8$  sec, which correspond to sampling the aircraft positions every  $8 \times 230 = 1840$  m, i.e. slightly less than 2 km.

In Fig. 2.5 we show the percentage of conflicts un-detected by the model for different values of  $\delta t$ . The percentage is computed with reference to the number of conflicts detected with  $\delta t = 1$  sec. With the  $\delta t = 8$  sec choice, we miss only  $\approx 0.2\%$  of conflicts. The red line corresponds to a 1% loss of conflicts, which would correspond to  $\delta t \approx 19$  sec.

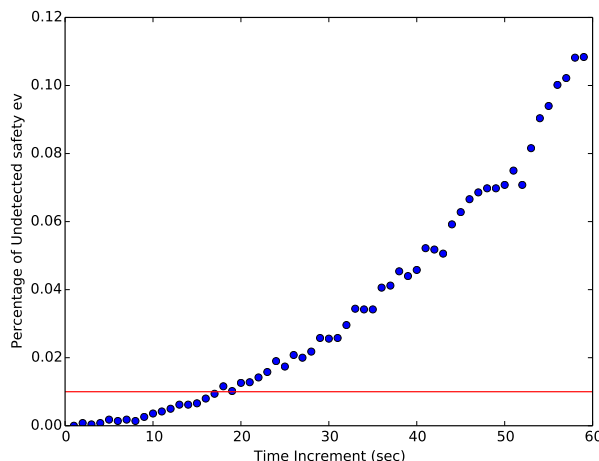


Figure 2.5: Percentage of conflicts un-detected by the model for different values of  $\delta t$ . The percentage is computed with reference to the number of conflicts detected with  $\delta t = 1$  sec. The red line corresponds to a 1% loss of conflicts

### 2.1.5 Performance

As mentioned above, the model was calibrated starting from data relative to the LIRR ACC (1763 flights). With these parameters, one single simulation takes 9 seconds.

In order to address what are the performance of the model in terms of computation time, we considered the same parameters and performed one single simulations over the whole Italian airspace (2453 flights). In this case one single simulation takes 13 seconds. We also performed a simulation on the whole ECAC airspace (9332 flights). In this case one single simulation takes 1 minute and 47 seconds.

These numbers were obtained starting from a machine with a Intel(R) Core(TM) i7-4700HQ CPU @ 2.40GHz processor with RAM 16Gb.

## 2.2 Validation of the Model Assumptions

This section describes the activities carried out to validate the model's assumptions with the aim to ensure that it is able to reproduce the current and the SESAR scenario in a realistic way, and that the parameters used are understandable from an operational point of view.

### 2.2.1 Validation Meeting

As defined in the deliverable *D4.4 - Validation Plan*, two of the main validation objectives related to the development of the SESAR Agent Based Model are:

- to build a Multi-sector ABM
- to simulate a realistic SESAR scenario

The achievement of these objectives has been assessed through validation activities carried out mainly as interviews with operational experts. In particular a validation meeting with the SESAR expert Dr. Fedja Netjasov, from the University of Belgrade, has been organized to illustrate him the features of the model and get his feedback in terms of the capability of the model to replicate real operational conditions and to simulate a realistic SESAR scenario. The validation was performed by presenting the model structure and by collecting his feedback through a set of questions defined around six main topics as follows:

- **INPUT to the MODEL** - In the model we have a few parameters that we can tune to generate different scenarios. Examples of these inputs are:

- The angle between planned and deviated trajectories;
- the pdf (probability density function) of departure times;
- the average velocity of aircraft;
- the controllers' look-ahead;
- the maximum vectoring angle;
- the preference of the controller to give directs or flight level changes or vectoring.

Are these parameters enough? Should we include anything else? Are these parameters enough clear from an operational point of view? Are these parameters enough close to operational concepts?

- **PRIORITIZATION** - In the model conflicts on the i-th aircraft are solved conditioned on the behaviour of the other (i-1) ones. This implies that we might not find the "optimal" solution, although we believe this is more similar to the ATCs operational conduct.

- Is this approach realistic from an operational point of view?

- **PREDICTIVE POWER OF THE MODEL** - What are the kind of things you expect to investigate with this model?

- **SECTORS**

- What are the relevant features that should be included in the multi-sector version of the model?
- What are pros and cons of having an airspace partitioned in sectors?

founding members



Avenue de Cortenbergh 100 | B- 1000 Bruxelles | [www.sesarju.eu](http://www.sesarju.eu)

33

- What are the good things about sectors (if any) that should be maintained in the SESAR scenario? Capacity is a relevant issue or not?
- Is local management of trajectories an issue that should be taken into account?

• **SESAR scenario**

- Are the features included in the model able to reproduce the SESAR scenario in a realistic way?
- Are there relevant features that should be included to increase the usefulness of the model results?
- Is the model correctly addressing the benefits foreseen for SESAR (D4.4)

• **CAPACITY STRESS TESTS**

- Where can be found reliable data on traffic forecasts?
- Is increasing the number of aircraft in a sector sufficient to perform capacity stress tests?

## 2.2.2 Expert's feedback

On the basis of the topics described in the previous section and related questions an overall positive feedback was obtained from Dr. Fedja Netjasov. In particular he appreciated the integration of the Strategic and Tactical layer and the possibility of feeding the model with conflict-free trajectories. More specifically the suggestions and comments received can be summarized as follows:

1. The parameters used in the model are sufficient for a realistic description of the current and the SESAR scenario. They are all clear from an operational point of view. However it has to be considered that a change of no more than 1000 feet, i.e. 10 FL, is used to avoid conflicts. In addition the velocity change can still be considered as a conflict resolution strategy in the SESAR scenario with planned conflict free trajectories.
2. The proposed approach, although different from reality, is reasonable and able to adequately mimic the way conflicts are handled by controllers.
3. The analyses expected to be carried out with the model are related to the number of action of the controllers, the number of resolved conflicts, (i.e workload) in nominal and non-nominal conditions in different scenarios.
4. The scope of the model should be broad. The model was presented as "multi-sector", but it seems that scope should be much broader to be able to cover even ECAC airspace. It is in fact more reasonable to consider the Free Route Airspace at a transnational level than at the level of a single FIR.
5. With respect to the capacity stress test the complexity of traffic situation should also be taken into account distinctly from number of aircraft. Critical number should be a number of aircraft which, under given circumstances (complexity), can not be safely handled anymore. Therefore critical number could be less than maximum number of aircraft handled. Data about traffic forecasts can be found on STATFOR website (<https://www.eurocontrol.int/statfor>).
6. In terms of benefits to the SESAR community, the model seems to have potential to provide more benefits than those already foreseen.

### 2.2.3 Addressing expert's feedback

The points raised during the validation meeting were analysed and addressed in the further development of the model. In particular the following changes/features have been implemented:

- The maximum flight level change was set according to comment 1. Regarding the use of velocity change to solve conflict, the dedicated module was already part of the model from the previous versions, see deliverable D2.3 [1]. However, we decided not to use it in the analyses shown in the present deliverable because, according to the feedback, it would have made sense using it only in the SESAR scenario. However, using different strategies for conflict resolution in the current and SESAR scenario could jeopardize the comparison of the results in the two cases.
- Analyses have been carried out considering the behaviour of the model in nominal and non-nominal conditions by measuring the metrics suggested in comment 3 such as the number of controllers actions.
- Although the model is designed to be extended up to ECAC level, as suggested in comment 4, due to computational issues it was not possible to carry out analyses at ECAC level. However analyses were carried out at ACC level on different FIRs.
- The 50% increase of traffic used in the capacity stress test was confirmed to be a value compatible (and even higher) with the forecasts on STATFOR and therefore reasonable to perform stress tests. However it was not possible to find information on the traffic forecasts per city-pairs to better tailor the capacity stress-tests. These information are not available on STATFOR.

## 3 Input Data Generation

In this chapter we describe the additional modules of the model that we used to generate the input data to the model necessary in order to perform the different simulations.

### 3.1 Flight Plan Generator 1 module: from M1 real trajectories

The first Flight Plan Generator produces M1 surrogate file starting from real data. In fact, for the considered day and for the considered airspace, we select the flight plans according to the filters illustrated in section 2.1 and then we generate surrogate flight plans that preserve:

- The distribution of flight between origin and destination. For an example, see the left panel in Fig. 3.1.
- The occupancy of flight levels (with odd rule). For an example, see the right panel in Fig. 3.1.
- The distribution of departure times. For an example, see green curve in Fig. 4.2 below.

The module requires as input the navigation point network that is generated starting from real data and produces surrogate M1 flight plans where each trajectory is the best-path on the navigation point network. The generated trajectories are therefore relative to the CURRENT scenario, by construction. One can use the rectification procedure of section 1.3.1 or the rectification procedure of section 1.3.2 to generate flight plans with larger efficiency up to the level of the SESAR scenario.

This module does not take into account capacity constraints. It will therefore be used in those simulations where we would like to emphasize the fact that in the SESAR scenario sectors will play a minor role.

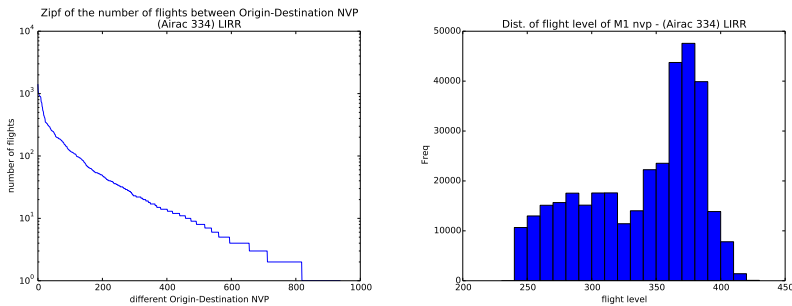


Figure 3.1: Empirical probability distribution of the number of flights between origin and destination airports (left panel) and empirical probability distribution of flight level occupancy in day 06/05/2010, LIRR ACC.

## 3.2 Flight Plan Generator 2 module: from M1 simulated trajectories

The strategic ABM presented in the deliverable D2.3 [1] has been used as a traffic generator in the present SESAR version of the ABM. An interface has been built so that the output of the strategic layer can be directly plugged into the present version of the ABM. The strategic ABM is included with all its features but an easy setup with default parameters fixed is provided, so that it can be used as a traffic generator pretty transparently. In the following we highlight the features which were not present in the previous version. For more details about how the strategic layer works, in particular the core module of the allocation of flights plans, the reader can refer to deliverable D2.3 [1].

The code is organized in several modules which can be used pretty much independently. The first module is the network generator, which has not been used for the present results, so we will skip its description. A description of an earlier version can be found in deliverable D2.3 and an updated one will be present in D2.5.

The second feature is the ability to feed the traffic generator with some data to extract independently:

- the distribution of altitudes
- the entry/exit points,
- the times of entrance,
- the capacities.

Hence, based on data provided by the ELSA database, we can generate some traffic matching exactly the data, or bootstrap the times of entrance, the entry/exit, etc. This allows to change some important parameters (for instance the number of flights) in a controlled way, by keeping different features of the original data.

Since we do not have access to the capacities directly in the database, they are inferred from traffic data. For this, we assume that all sectors reach their capacities at some point in time. Hence, the maximum occupancy detected based on the traffic is set as capacity. This allows to have the differences of capacity between different sectors. In a next step, we set a target for the number of flights rejected and scale down the capacity uniformly so as the fraction of rejected flights matches the target. The capacities can then be used by the tactical ABM for its own purposes, see section 1 (multi-sector module).

The next module is the allocation module, which is the core of the strategic model. In short, it mimics the submission of flights plans from air companies to the CFMU network manager, which can refuse to allocate a flight if some capacities are overreached. As output, this module gives 2+1d trajectories which are compliant with the given capacities.

Since the strategic ABM is a model in 2+1-D, whereas the tactical is fully in 3+1-D, we have written some automatic procedures in a third module to generate some synthetic altitudes in a comprehensive way. Different options of altitude generation are implemented, including:

- Fully random altitudes,
- user-given analytical distribution,
- distribution extracted from data.

These distribution are used for the starting and ending altitudes in the area. Then we produce surrogate trajectories by randomly selecting fully increasing, fully descending or ascending then descending profiles. Note that these profiles are linear and thus might be unrealistic in this respect. Moreover, we enforce the 180° rule which stipulates that flights going roughly from East to West and those going from West to East are separated by 10 FL.

In section 4 we have used the third option for the generation of altitudes, i.e. the distribution extracted from data. The data comes from the ELSA database for the chosen airspace.

The generated trajectories are relative to the CURRENT scenario, by construction. One can use the rectification procedure of section 1.3.2 or the rectification procedure of section 1.3.1 to generate flight plans with larger efficiency up to the level of the SESAR scenario. However, it should be emphasized that when generating flight plans with larger efficiency, the capacity constraints will not be modified. Therefore we will have an hybrid situation where we consider flight plans with enhanced efficiency and with capacity constraints that are still those of the current scenario.

As a final remark, we want to emphasize that we also use a slightly different procedure to generate the flight-plans with respect to the one of section 3.1. In fact, in 3.1 we consider the shortest path between origin and destination on the considered navigation points network, while in general this is not true in this module.

### 3.3 Pre-tactical de-conflicting module

The deconflicting module we describe here takes as input M1 real or surrogate trajectories. In other words, we start from M1 flight plans and try to make them conflict-free by using a *brute force* method.

In fact, it is assumed that in the SESAR scenario, differently from the current scenario, the flight-plan recorded in the M1 files will already be conflict-free, due to a better strategic planning of the different aircraft trajectories. Therefore in order to eliminate any possible bias due to this issue we decided that in some case it might be worth to consider M1 de-conflicted trajectories for all the networks with different efficiency values generated by using the procedures of section 1.3.

Specifically, we use the Conflict Detection Module of section 1.2 to detect possible conflicts. Starting from M1 files, we consider all flight trajectories active in the selected ACC and in the considered day. If a conflict is detected, we randomly shift in time the departure of the interested aircraft of an amount of time within the range [-5 min, 5 min]. We try this procedure until the flight trajectory is de-conflicted, for a maximum number of 100 iterations. If at the end of the 100 iterations the aircraft is still involved in a safety event we try to shift in time the departure of this aircraft of an amount of time within the range [-10 min, 10 min], then within the range [-15 min, 15 min] and finally in the range [-20 min, 20 min].

At the end of this process all M1 flight trajectories will be conflict-free. Indeed, in a few cases even enlarging the shift time interval to 20 min may be not enough to get conflict-free M1 flight trajectories. In this case, we start again the procedure starting from another flight-plan.

This module may be switched on and off, depending on the type of simulations we want to perform.

## 4 Results

We model the flights trajectories within a set of 15 ACCs: LFFF, EGpx, LECB, LFMM, LECM, LECS, LFRR, LIPP, LECP, EGCC, LIMM, LFEE, EGTT, LIBB, LIRR. The main features of these ACCs are reported in Table 4.1.

ACC	ACC name	number of flights	Area (km <sup>2</sup> )	Number of sectors
LIRR	<b>Rome</b>	2122	501732	10
LIMM	Milan (I)	1066	73234	5
LIPP	Padova (I)	1083	95360	5
LIBB	Brindisi (I)	448	244179	3
LFFF	<b>Paris</b>	639	171702	4
LFMM	Marseille (F)	1494	299525	11
LFEE	Reims (F)	1799	98989	5
LFRR	Brest (F)	1886	400217	11
EGTT	<b>London</b>	2854	3648975	18
EGCC	Manchester (UK)	786	47959	3
EGpx	Scotland	614	6838031	12
LECM	<b>Madrid</b>	2203	442101	10
LECB	Barcelona (ES)	1366	266783	9
LECP	Palma (ES)	321	51173	6
LECS	Sevilla (ES)	660	182051	15

Table 4.1: Main features of the 15 considered ACCs.

In Fig. (4.1) we give a simplified graphical representation of how a simulation looks like at a certain time. The green lines represent the M1 flight-trajectories. The blue circles represent the aircraft active in the sector at that time instant in the central flight level. The magenta circles represent the aircraft active in the sector at that time instant in the lower or higher flight level. The red spot represents a shocked area. The circles representing the aircraft have a radius equal to 2.5 Nautical miles. This is half of the minimum distance at which aircraft can pass close to each other without generating a safety alarm. In the figure one can see that the rightmost aircraft in blue is slightly moving away from its M1 trajectory. In fact, it is starting to modify its trajectory in order to overcome the incoming shocked area in red.

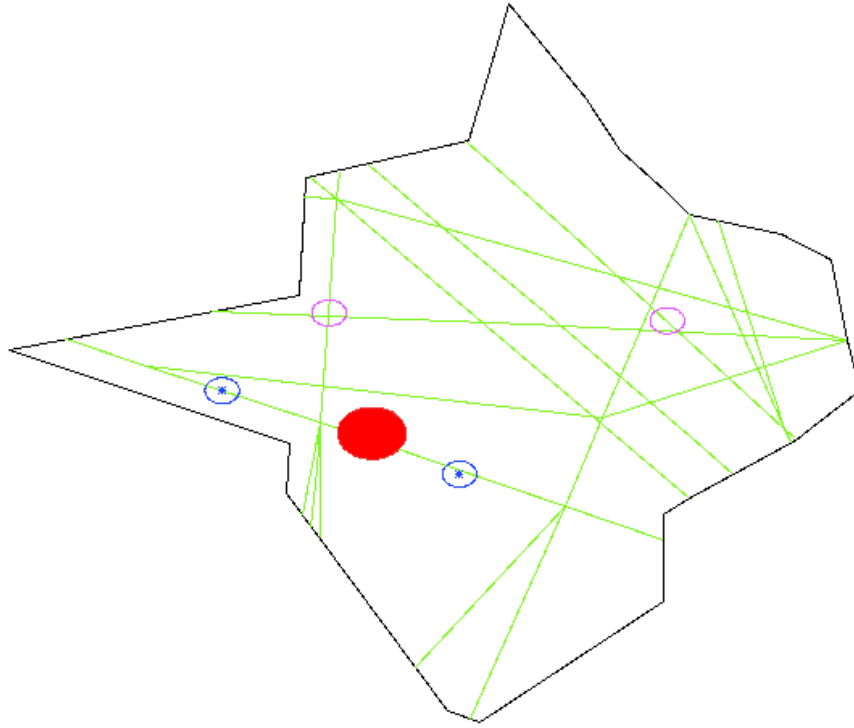


Figure 4.1: Simplified graphical representation of a simulation at a certain time. The green lines represent the M1 flight trajectories. The blue circles represent the aircraft active in the sector at that time instant in the central flight level. The magenta circles represent the aircraft active in the sector at that time instant in the lowest or highest flight level. The red spot represents a shocked area.

The conflict resolution module only performed re-routings and flight-level changes. The submodule of section 1.2.6.3 was switched off.

## 4.1 Results on a single ACC: capacity stress-test

We performed a first set of simulations by using the rectification procedure of section 1.3.1 and the Conflict-Free Flight Plan Generator of section 3.1. The aim of this test is to discover which network, in terms of efficiency, is more resilient to a small perturbation of the initial conditions. In this set of simulations the perturbation is the delay on departure.

Due to the high computational effort needed by the Conflict-Free Flight-Plan Generator of section 3.1, we considered just one ACC: the Italian LIRR. We considered 20 values of efficiency, ranging from the real LIRR efficiency  $E=0.9729$  up to  $E=1$ . We considered the M1 flight trajectories relative to day 06/05/2010 of the 334 AIRAC and we de-conflicted them by using the module of section 3.3. In Fig. 4.2 we show that the de-conflicting procedure (blue line) does not significantly alter the distribution of time departure with respect to the one observed in the original M1 flights (green line).

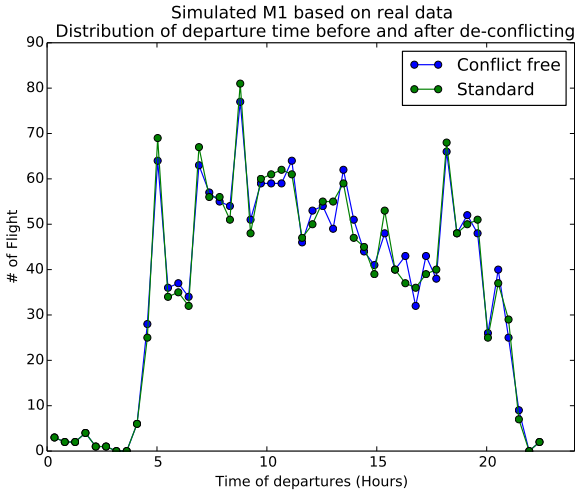


Figure 4.2: Distribution of time departure for the de-conflicted (blue line) and original M1 flight trajectories (green line).

After the M1 trajectories were pre-tactically de-conflicted, for each value of efficiency we performed 10 simulations. In each simulation we perturbed each flight trajectory by randomly assigning a delay on departure to a percentage  $f_d$  of the flight trajectories. The maximum amount of delay on departure was  $d_{max} = 600$  sec and the percentage of delayed flight trajectories was  $f_d = 0.20$ . Finally the simulation has been performed for an increasing number of aircrafts present in the ACC, ranging from  $N_f = 1500$  to  $N_f = 2200$ .

In Fig. 4.3 we show the average number of conflicts detected in the LIRR ACC, for different values of efficiency (horizontal axis) and for different values of the aircrafts present in the ACC (different lines in the plot). Each of the shown curves has been normalized with  $N_f^2$ , i.e. with the maximum possible number of conflicts in an environment with  $N_f$  aircraft. The average number of conflicts is here measured as the average number of actions that the controller has to perform in order to avoid the conflicts detected by the Collision Module of section 1.2. Therefore, these measures are performed on the surrogate M3 flight trajectories generated by our model. Indeed, the figure shows two interesting features: on one side we have that all curves seem to collapse in a single curve when the number of conflicts is rescaled with  $N_f^2$ . The second interesting feature is that the number of detected conflict diminishes as long as efficiency increases, thus indicating that in the SESAR scenario we should observe less conflicts and therefore a smaller workload for controllers.

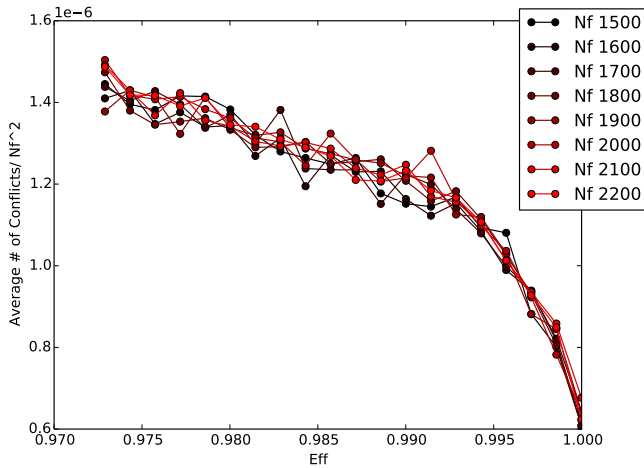


Figure 4.3: Average number of conflicts detected in the surrogate M3 flight trajectories of the LIRR ACC, for different values of efficiency (horizontal axis) and for different values of the aircrafts present in the ACC (different lines in the plot). Each of the shown curves has been normalized with  $N_f^2$  that represents the maximum possible number of conflicts in an environment with  $N_f$  aircraft.

We have also devised a simple procedure to compute what is the expected number of possible safety events (PSE) we should expect. In this way, we can assess whether the results of Fig. 4.3 are realistic or not. We start from the M1 de-conflicted trajectories and implement the following procedure:

- we perform a very fine spatial sampling of all flight trajectories. Sample points are distant 1 meter one from each other.
- starting from the original flight plans we associate to each of these sampled points a timestamp. This is done by assuming that between two navigation points the velocity of the aircraft is constant.
- we select those sampled points  $P_i^{(f_1)}$  in the  $f_1$ -th flight trajectory and  $P_j^{(f_2)}$  in the  $f_2$ -th flight trajectory such that the Euclidean distance  $d(P_i^{(f_1)}, P_j^{(f_2)})$  between the two points is smaller than the safety threshold distance  $d_{thresh} = 5$  NM.
- we further select those points such that the times  $t_i^{(f_1)}$  at which the  $f_1$ -th aircraft crosses  $P_i^{(f_1)}$  and  $t_j^{(f_2)}$  at which the  $f_2$ -th aircraft crosses  $P_j^{(f_2)}$  are below a certain time threshold  $T_{thresh}$ .

By using such procedure we are able to show what are the points of the ACC that are likely to attract the controller attention as a source of possible safety events. Of course, the PSEs thus defined are strictly depending on the  $T_{thresh}$  considered. In Fig. 4.4 we show the PSEs detected in the LIRR ACC, for different values of efficiency (horizontal axis) and for different values of the aircrafts present in the ACC (different lines in the plot). Each of the shown curves has been normalized with  $N_f^2$ , i.e. with the maximum possible number of conflicts in an environment with  $N_f$  aircraft. In the figure we show the results for  $T_{thresh} = 5.0$  min although we performed such analyses for different values of  $T_{thresh}$ . Also in this case, the figure shows two interesting features: on one side we have that all curves seems to collapse in a single curve when the number of conflicts is rescaled with  $N_f^2$  and

the number of detected conflict diminishes as long as efficiency increases, thus indicating that in the SESAR scenario we should expect less conflicts and therefore a smaller workload for controllers.

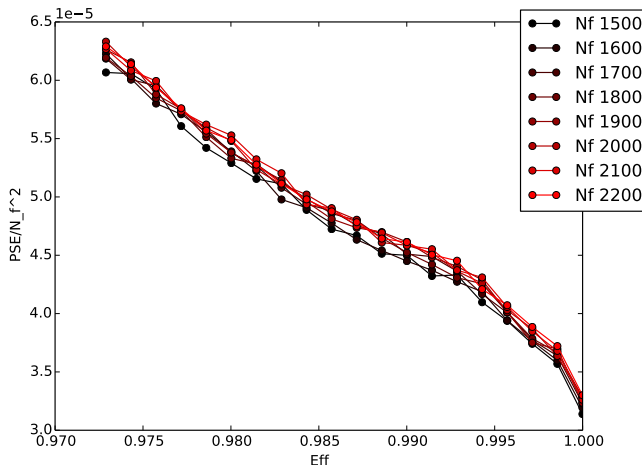


Figure 4.4: Average number of possible safety events (PSE) detected in the M1 flight trajectories of the LIRR ACC, for different values of efficiency (horizontal axis) and for different values of the aircrafts present in the ACC (different lines in the plot). Each of the shown curves has been normalized with  $N_f^2$  that represents the maximum possible number of conflicts in an environment with  $N_f$  aircraft.

The analysis of PSE is quite time consuming from a computational point of view. The evaluation of the distance is the most lengthy operation. We decided to use the Euclidean distance rather the Haversine distance in order to reduce the computational effort. This approximation can be justified when working at the level of ACC. in fact, in Fig. 4.5 we show a comparison between the number of actions done by the controllers when we implement the Haversine distance (red) and the Euclidean distance in the LIRR ACC. The agreement between the two curves is within the error bars. These curves are obtained by considering 10 simulations in which 70% of aircraft is randomly delayed by a maximum of 5 min and the ABM is working in the current scenario. The time needed to perform one simulation with the Haversine distance is 10.7 sec, while considering the Euclidean distance we go down to 4.2 sec. When working on a larger airspace using the Euclidean distance might produce incorrect estimations.

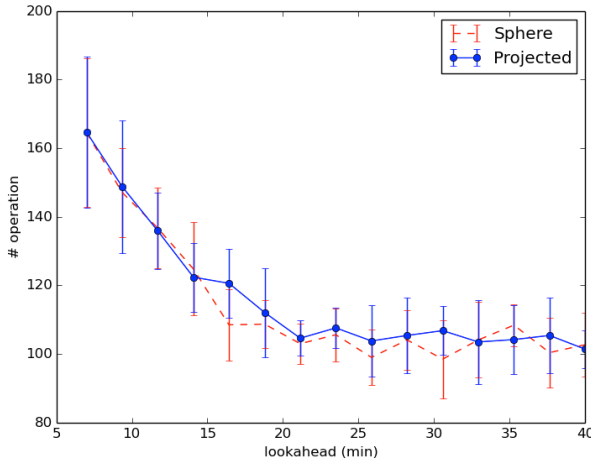


Figure 4.5: comparison between the number of actions done by the controllers when we implement the Haversine distance (red) and the Euclidean distance in the LIRR ACC. These curves are obtained by considering 10 simulations in which 70% of aircraft is randomly delayed by a maximum of 5 min and the ABM is working in the current scenario. The time needed to perform one simulation with the Haversine distance is 10.7 sec, while considering the Euclidean distance we go down to 4.2 sec.

In Fig. 4.6 we show a scatter-plot between the normalized PSEs detected from the M1 files with  $T_{thresh} = 5.0$  min (horizontal axis) and the normalized number of conflicts detected from the surrogate M3 files (vertical axis) for different values of efficiency. The figure shows the existence of two different regimes. For values of efficiency close to unity the curve can be fitted with a linear relationship whose slope is of the order of 0.05, while for lower values of efficiency we have a linear relationship whose slope is of the order of 0.01. In any case, the fact that the curve is steeper for high values of efficiency indicates that a small variation in the PSEs translates into a larger variation of the number of detected conflicts, thus indicating that the SESAR scenario might reveal to be less flexible to accommodate variation in the planning of the trajectories.

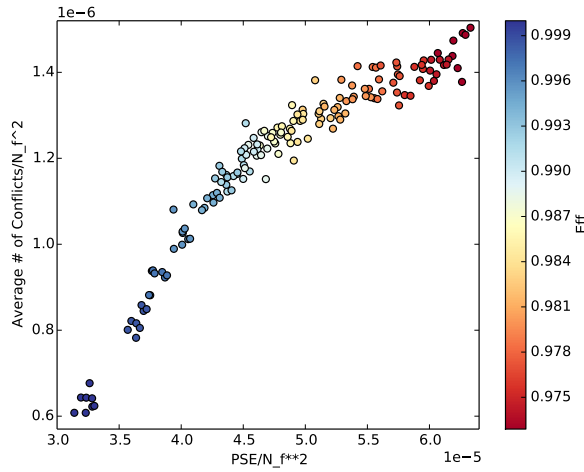


Figure 4.6: Scatter Plot of the average number of conflicts detected in the surrogate M3 flight trajectories versus the average number of possible safety events (PSE) of the LIRR ACC. Different points represent different values of efficiency and different values of the aircrafts present in the ACC.

In Fig. 4.7 we show a density map of the PSEs detected when considering three different values of efficiency and  $T_{thresh} = 5.0$  min. In the left panel we show the PSEs detected starting from the real M1 trajectories, which corresponds to an efficiency value of  $E = 0.9729$ . In the right panel we show the PSEs detected starting from the M1 trajectories corresponding to the SESAR scenario, i.e. with an efficiency value of  $E = 0.99999$ . In the central panel we show the PSEs detected starting from the M1 trajectories corresponding to the intermediate value of efficiency  $E = 0.9800$ . As expected, as long as efficiency increases the possible conflicts are more spread all over the ACC, rather than being concentrated in specific regions. This might explain why the number of detected conflicts diminishes as long as efficiency increases. This also implies that the controller activity in the SESAR scenario will change, moving from a situation where he has to give attention to an high number of conflicts concentrated in specific points to a situation where he will have to manage less conflicts spread in a much larger portion of the airspace.

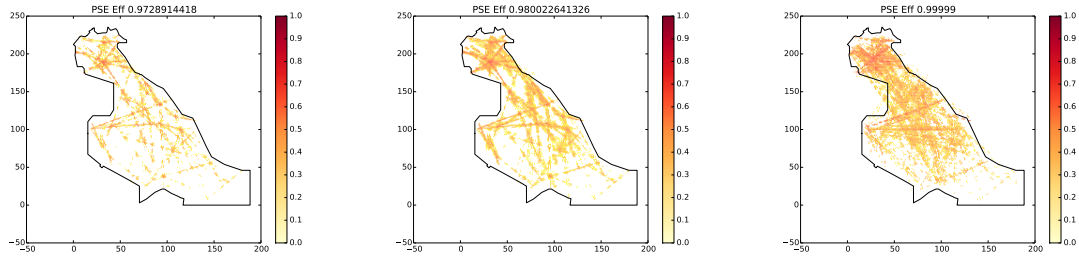


Figure 4.7: Density map of the PSEs detected when considering three different values of efficiency and  $T_{thresh} = 5.0$  min in the LIRR ACC. In the left panel we show the PSEs detected starting from the real M1 trajectories, i.e. of  $E = 0.9729$ . In the right panel we show the PSEs detected starting from the M1 trajectories corresponding to the SESAR scenario, i.e. with an efficiency value of  $E = 0.9999$ . In the central panel we show the PSEs detected starting from the M1 trajectories corresponding to the intermediate value of efficiency  $E = 0.9800$ . To enhance readability, we first take the logarithm of the number of PSEs and then we normalize by dividing all logarithms by the maximum one.

## 4.2 Results on different ACCs

We performed a second set of simulations by using the rectification procedure of section 1.3.2 and the Conflict-Free Flight Plan Generator of section 3.2. The aim of this test is the same as in section 4.1. However, in this case we decided to consider many different ACCs in order to investigate whether the results obtained in section 4.1 might depend on the features of the starting network of navigation points. Also in this case, we here considered as a starting point the real data relative to AIRAC 334 and day 06/05/2010. Again, we want to emphasize that we also use a slightly different procedure to generate the flight-plans with respect to the ones used in section 4.1. In fact, in section 4.1 we used the Conflict-Free Flight Plan Generator of section 3.1 which makes use of the shortest path route on the considered navigation points network, while here we instead consider the Conflict-Free Flight Plan Generator of section 3.2 based on the real planned trajectory, which not always corresponds to a shortest path.

By using the Conflict-Free Flight Plan Generator of section 3.2, for each ACC we generated 100 surrogate M1 flight plans preserving four stylized facts observed in the real M1 files:

- The distribution of departure times.
- The distribution of flight levels for each navigation point (also with the constraint of the odd rule),
- The same fraction of number of flights between each origin-destination pair.
- The same total number of flights in the ACC.

After generating such virtually de-conflicted M1 trajectories, for each ACC we performed 10 simulations. In each simulation we perturbed each flight trajectory by randomly assigning a delay on departure to a percentage  $f_d$  of the flight trajectories. The maximum amount of delay on departure was  $d_{max} = 600$  sec and the percentage of delayed flight trajectories was  $f_d = 0.20$ .

Furthermore, we performed two types of simulation. The first one was made without the direct modules (i.e.  $p_d = 0$ ), the second one with the direct module with  $p_d = 1$ . This is done because we want to investigate the extreme situation occurring when either we do not have directs or a direct is

ACC	original efficiency	target efficiency 1	target efficiency 2	target efficiency 3
EGTT	0.9145	0.954	0.98	0.999
LIMM	0.9278	0.954	0.98	0.999
LIRR	0.9448	0.98	0.999	
LFRR	0.9509	0.98	0.999	
LFFF	0.9524	0.98	0.999	
EGPX	0.9550	0.98	0.999	
LECP	0.9623	0.98	0.999	
LECM	0.9744	0.999		
LECS	0.9751	0.999		
LECB	0.9756	0.999		
LFMM	0.9781	0.999		
LFEE	0.9813	0.999		
EGCC	0.9848	0.999		
LIBB	0.9849	0.999		
LIPP	0.9850	0.999		

Table 4.2: Efficiencies values used in the numerical simulations for the 15 ACCs. Such values have been obtained starting from the data relative to AIRAC 334 and day 06/05/2010. The efficiency value for LIRR is different from the one used in section 4.1, due to the fact that the Conflict-Free Flight Plan Generator of section 3.1 considers shortest paths, while the Conflict-Free Flight Plan Generator of section 3.2 considers real trajectories.

issued whenever it is possible. For each of the 15 ACCs mentioned above we made simulations for its real efficiency value (current scenario) and the ideal unitary efficiency value corresponding to the SESAR scenario. In a few cases we also considered intermediate values of efficiency. The considered cases are summarized in Table 4.2. In the table, all ACCs are ordered according to their original efficiency value.

In Fig. 4.8, for each of the 15 ACCs and in the two extreme cases of  $p_d = 0$  (blue circles) and  $p_d = 1$  (red circles), we show a scatter-plot of the efficiency obtained after running the ABM versus the original efficiency measured in the ACC. In both cases, there exists a linear relationship between the M3 and the M1 efficiency. However, the efficiency obtained by issuing a direct is larger than the one obtained by generating flight trajectories where no direct is issued. Such result is of course expected. The importance of these two curves lies in the fact that they constitute the boundaries between which our simulations will have to stay.

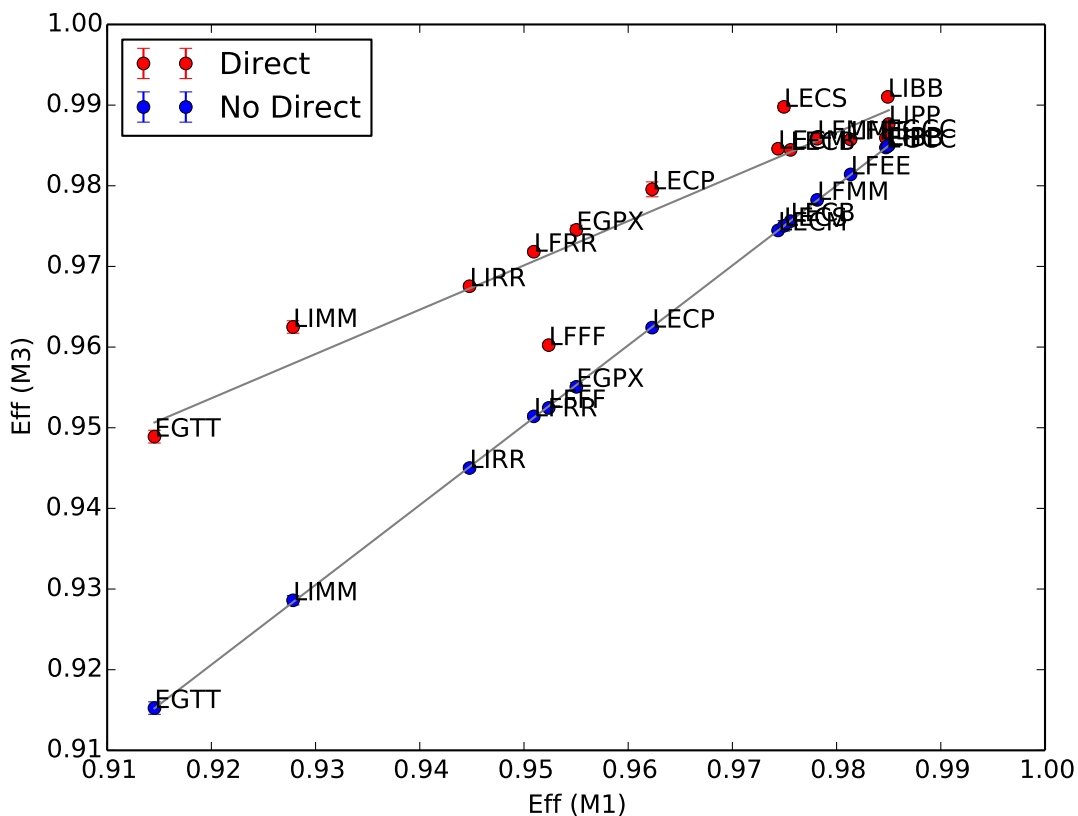


Figure 4.8: Scatter-plot of the efficiencies of the M3 surrogate trajectories obtained after running the ABM versus the original efficiency measured for each of the 15 ACCs and in the two extreme cases of  $p_d = 0$  (blue circles) and  $p_d = 1$  (red circles).

In Fig. 4.9 we show a scatter-plot of the efficiency obtained after running the ABM versus the original efficiency for all the 39 target efficiencies of Table 4.2 and in the two extreme cases of  $p_d = 0$  (blue circles) and  $p_d = 1$  (red circles). Remarkably, all 30 points with  $E = 0.999$ , i.e. for all 15 ACCs with  $p_d = 1$  and  $p_d = 0$ , are essentially coincident, see right panel of the Figure. This would indicate that in the SESAR scenario giving directs has no role because trajectories are already rectified. We take this result as a check of internal consistency and as an indication of the fact that issuing directs and performing a rectification of trajectories ends up in the same scenario.

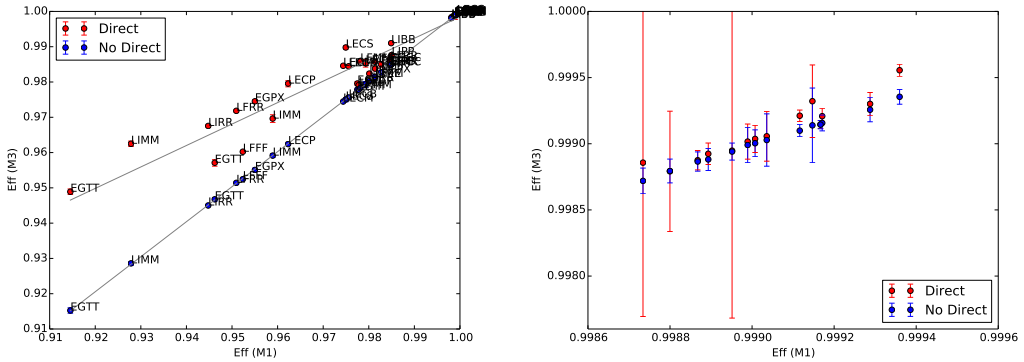


Figure 4.9: Scatter-plot of the efficiencies of the M3 surrogate trajectories obtained after running the ABM versus the original efficiency for all the 39 target efficiencies of Table 4.2 and in the two extreme cases of  $p_d = 0$  (blue circles) and  $p_d = 1$  (red circles). The right panel is a zoom of the region around  $E = 0.9999$ .

In Fig. 4.10, for each of the 15 ACCs and in the two extreme cases of  $p_d = 0$  (right panels) and  $p_d = 1$  (left panels), we show the number of re-routing (top panels) and the number of flight level changes (bottom panels) for the 15 ACCs. In this case we considered the original navigation points networks with their efficiency and the networks obtained by using the rectification procedure of section 1.3.2 with a few new target efficiencies. The figures show that in all cases the number of re-routing decreases as long as efficiency increases. However, the number of flight level changes might increase in some cases. In the bottom panels we show the total number of actions done by the ABM, i.e. we consider both re-routings and flight level changes. In this case, we number of actions generally decreases as long as efficiency increase, as already observed in Fig. 4.3.

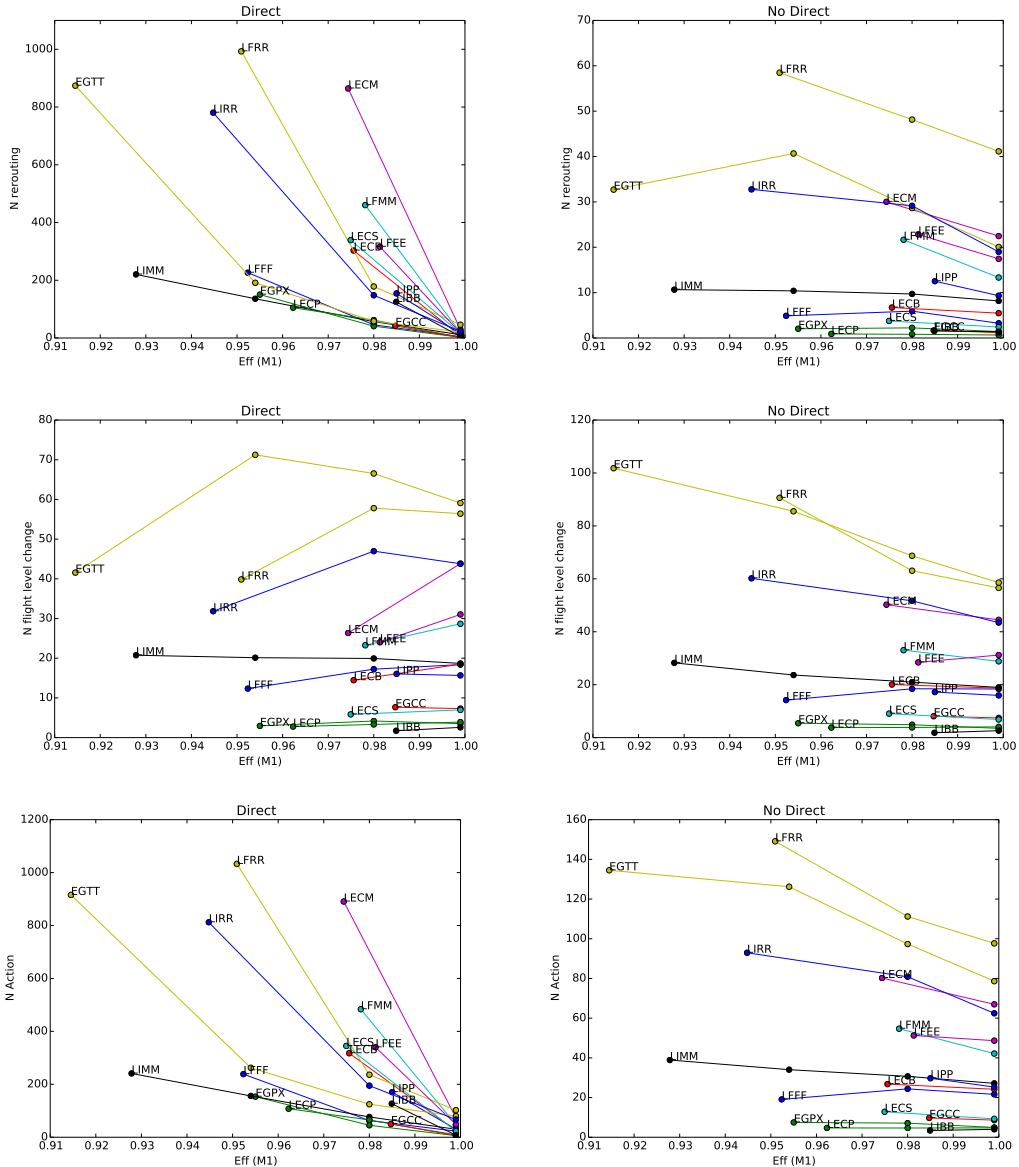


Figure 4.10: Number of re-routings (top panels) and number of flight level changes (central panels) and total number of actions (bottom panels) for each of the 15 ACCs and in the two extreme cases of  $p_d = 0$  (right panels) and  $p_d = 1$  (left panels).

For each of the 15 ACCs, let us consider the Gain metric defined as:

$$G = \frac{N(E_S) - N(E_C)}{N(E_C)} \quad (4.1)$$

where  $E_S = 0.9999$  is the target efficiency relative to the SESAR scenario and  $E_C$  is the efficiency of the considered ACC in the current scenario.  $N$  here indicates the number of re-routing actions done by the ABM. The G metric should indicate how much, in percentage, we gain in terms of number of

re-routings when we move from the current to the SESAR scenario. In Fig. 4.11 we show the Gain for the case when  $p_d = 1$  (top panel) and  $p_d = 0$  (bottom panel). As expected the Gain is larger when directs can be issued. However we were not able to see any dependance of the gain  $G$  from variables such as the original efficiency  $E_C$  or other ACC metrics as those reported in Table 4.1.

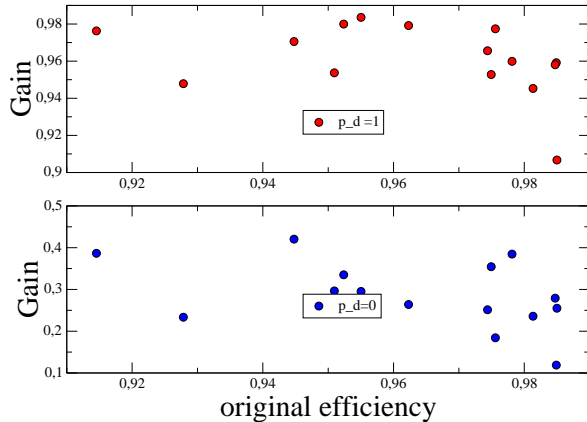


Figure 4.11: Gain metric of Eq. 4.1 computed for each of the 15 ACCs and in the two extreme cases of  $p_d = 0$  (bottom panel) and  $p_d = 1$  (top panel).

In Table 4.3 we show the average number of reroutings and flight level changes in the SESAR scenario ( $E=1$ ) for the two extreme cases  $p_d = 0$  and  $p_d = 1$ . The correlation between flight level changes and re-routings is 0.85 when  $p_d = 1$  and 0.80 when  $p_d = 0$ . The values of re-routings and flight level changes are quite similar in the two cases when  $p_d = 0$  and  $p_d = 1$ , thus indicating that trajectories are really linearized in the SESAR scenario and therefore issuing directs does not play a big role, as already notice in Fig. 4.8.

In Fig. 4.12 we show the number of re-routings versus the number of flight level changes for the case  $p_d = 1$  (left panel) and the when  $p_d = 0$  (right panel). In the figure the blue points correspond to the 15 ACCs considered with their original efficiency values, i.e. the one corresponding to the scenario (see Table 4.2). The figure indicates the existence of a positive correlation between number of re-routings and number of flight level changes, although there seems to exist no linear relation between the two variables. In fact, we observe a correlation of 0.879 for the current scenario when  $p_d = 1$  and 0.908 for the current scenario when  $p_d = 0$ . The lack of a linear law indicates that the starting navigation points network and the other metrics such as those of Table 4.1 might play a role. The red points correspond to the 15 ACCs considered with their unitary efficiency values, i.e. the one corresponding to the SESAR scenario. Also in this case a positive correlation between number of re-routings and number of flight level changes. For the SESAR scenario we observe a correlation of 0.840 when  $p_d = 1$  and 0.910 when  $p_d = 0$ . Moreover, in the SESAR scenario when  $p_d = 1$  we observe an increase on flight level changes and a decrease of the number of re-routings, while in the case when  $p_d = 0$  the differences between future SESAR and current scenario are negligible. This goes in the direction by which the rectification of trajectories (with direct, in this case) is again beneficial for the general efficiency of the system. The green points correspond to the intermediate values of efficiency reported in Table 4.2.

ACC	original efficiency	average number of reroutings (no directs)	average number of flight level changes (no directs)	average number of reroutings (directs)	average number of flight level changes (directs)
LFFF	0.9524	3.248	18.74	4.537	18.392
EGPX	0.9550	1.432	3.5	2.471	3.525
LECB	0.9756	5.477	18.693	6.846	18.508
LIPP	0.9850	9.326	15.953	14.414	15.672
LFEE	0.9813	17.447	31.207	17.288	31.028
LECM	0.9744	22.469	44.493	29.752	43.817
LFRR	0.9509	41.137	56.547	45.975	56.419
LECS	0.9751	2.423	6.844	16.014	6.981
LFMM	0.9781	13.326	28.829	18.473	28.672
LECP	0.9623	0.661	4.059	2.186	3.913
EGCC	0.9848	1.198	7.434	1.765	7.304
LIMM	0.9278	8.169	18.977	11.485	18.695
EGTT	0.9145	20.062	58.569	20.731	59.093
LIBB	0.9849	1.372	2.621	5.11	2.581
LIRR	0.9448	18.985	43.458	22.993	43.804

Table 4.3: fedja2

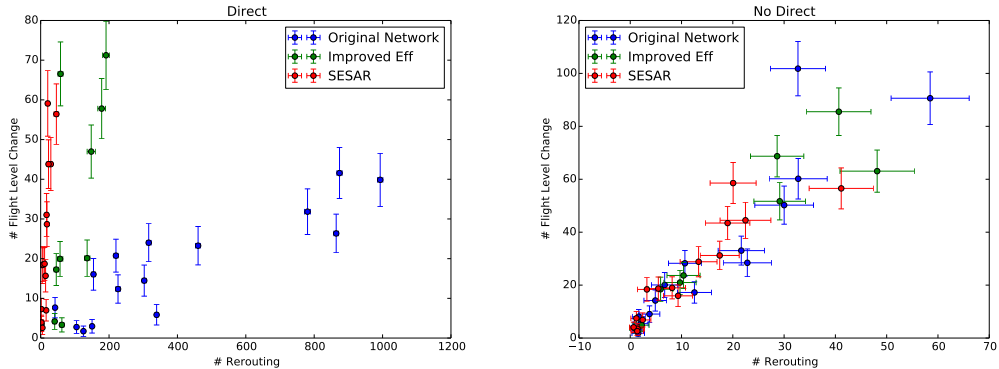


Figure 4.12: Scatter-Plot of the number of flight level changes versus the number of re-routings. The blue points correspond to the 15 ACCs considered with their original efficiency values, i.e. the one corresponding to the scenario. The red points correspond to the 15 ACCs considered with their unitary efficiency values, i.e. the one corresponding to the SESAR scenario. The green points correspond to the intermediate values of efficiency reported in Table 4.2.

In Fig. 4.13 we show the number of re-routings with respect to the number of flights in the ACC for the case  $p_d = 1$  (left panel) and when  $p_d = 0$  (right panel). The blue points correspond to the 15 ACCs considered with their original efficiency values, i.e. the one corresponding to the scenario. The red points correspond to the 15 ACCs considered with their unitary efficiency values, i.e. the one corresponding to the SESAR scenario. The green points correspond to the intermediate values of efficiency reported in Table 4.2. The relationship between number of re-routings and number of flights is approximatively linear. However, we recall that in Fig. 4.3 we had observed that the number of re-routings might rescale with  $N_f^2$ . In fact, the two empirical facts are not contrasting

with each other. Indeed, in Fig. 4.3 we were considering a given ACC with an arbitrarily changing number of flights. In the present case, we are considering different ACCs each with its own number of flights. Moreover, when looking at the points relative to the SESAR scenario with  $p_d = 0$  we do not see any clear relationship between number of re-routings and number of flights in the ACC, thus indicating that the specific features of the ACC might still play a role in the SESAR scenario. This is in a sense unfortunate. Had we observed a common behaviors in all ACCs in the SESAR scenario, this would have been a strong support to the idea of having more standard management procedures in the SESAR scenario. As shown in Fig. 4.14 similar considerations can be done for the relationship between number of flight level changes and number of flights in the ACC.

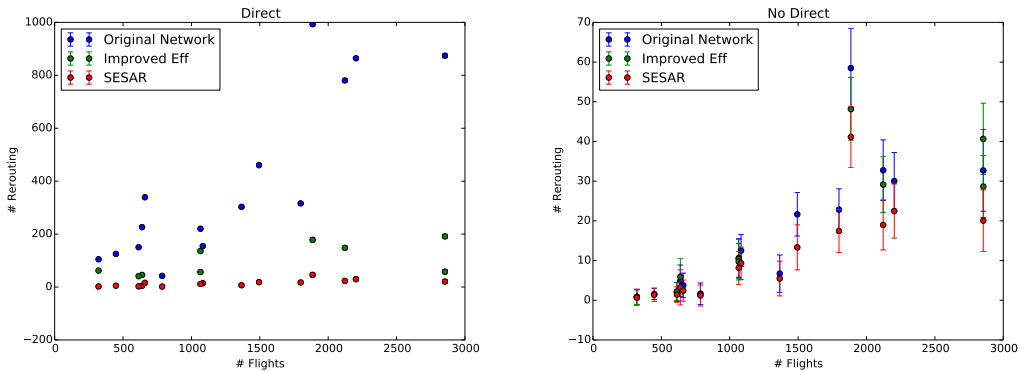


Figure 4.13: Number of re-routings as a function of the Number of Flights. The blue points correspond to the 15 ACCs considered with their original efficiency values, i.e. the one corresponding to the scenario. The red points correspond to the 15 ACCs considered with their unitary efficiency values, i.e. the one corresponding to the SESAR scenario. The green points correspond to the intermediate values of efficiency reported in Table 4.2.

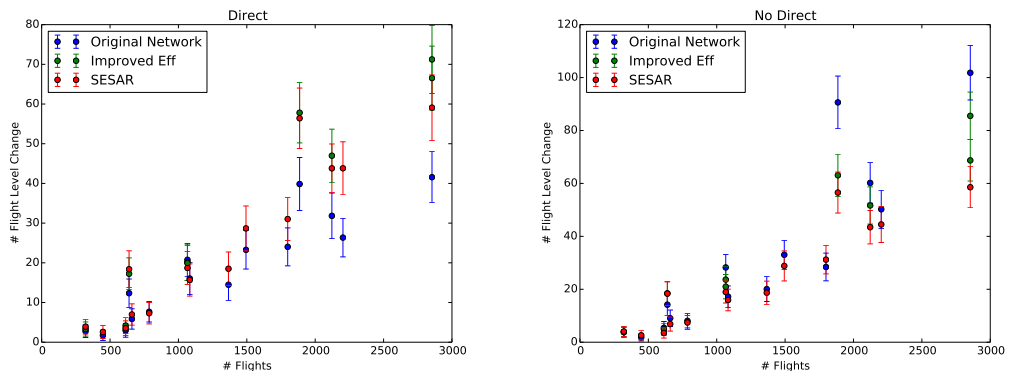


Figure 4.14: Number of Flight level changes as a function of the Number of Flights. The blue points correspond to the 15 ACCs considered with their original efficiency values, i.e. the one corresponding to the scenario. The red points correspond to the 15 ACCs considered with their unitary efficiency values, i.e. the one corresponding to the SESAR scenario. The green points correspond to the intermediate values of efficiency reported in Table 4.2.

In Fig. 4.15 we show the distribution of the number of re-routings for a few selected values of

efficiency in the case when we issue directs (right panel) and in the case when  $p_d = 0$  (left panels). As indicated in Table 4.2, we have a total number of 39 distributions in each of the two cases. In the case when we issue directs ( $p_d = 1$ ) 35 out of 39 distributions are gaussian distributions according to the Anderson-Darling statistical test [10]. In the case when there are no directs ( $p_d = 0$ ) only 21 out of 39 distributions are gaussian distributions according to the Anderson-Darling statistical test. In the Figure, we draw a reference gaussian distribution with mean and variance taken from observed data in the case when  $p_d = 1$ . When  $p_d = 0$  in the Figure we draw a reference Poisson distribution with mean and variance taken from observed data. The existence of a Gaussian distribution ensures that on average the probability that a controller has to perform a large number of actions remains low.

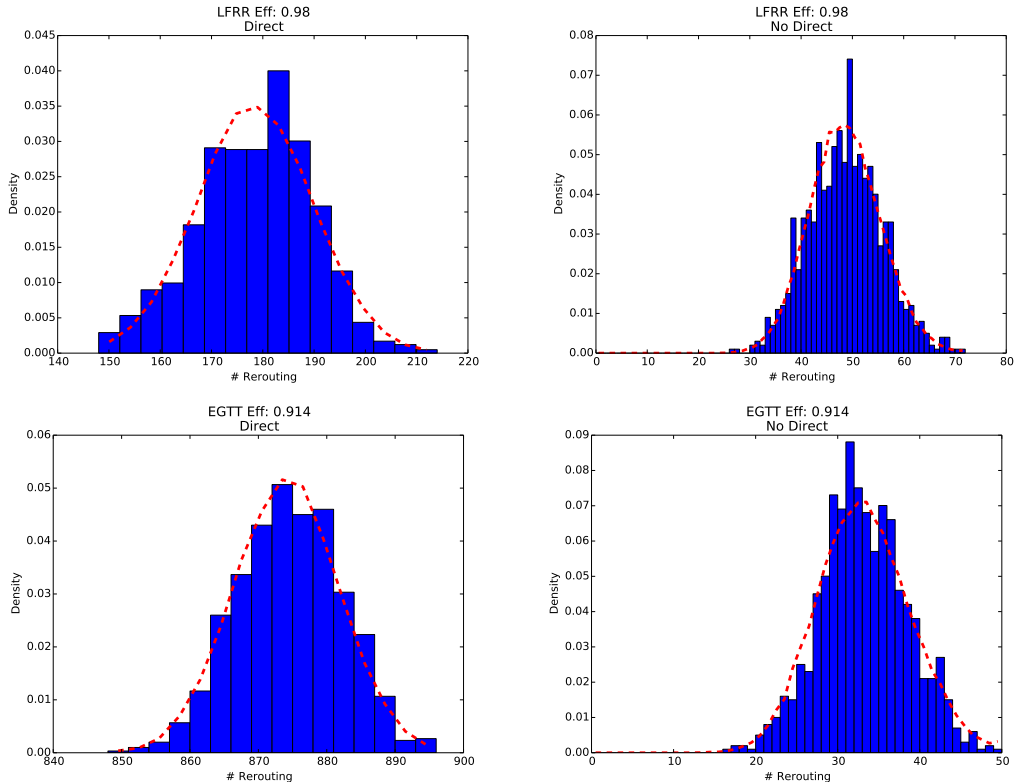


Figure 4.15: Distribution of the number of re-routings for a few selected values of efficiency in the case when we issue directs (right panel) and in the case when  $p_d = 0$  (left panels). The red lines correspond to a reference gaussian distribution with mean and variance taken from observed data in the case when  $p_d = 1$  and to a reference Poisson distribution with mean and variance taken from observed data when  $p_d = 0$ .

Finally, in Table 4.4 we show a summary statistics of the difference between the length of the M1 trajectories and the surrogate M3 trajectories for the current and SESAR scenario with and without shocks. Data refer to the LIRR ACC and are given in kilometers. The differences in the trajectory lengths are negligible in the SESAR scenario, thus indicating an overall increase of the M1 flight-plans predictability.

scenario	average	standard-deviation	min	max
current scenario $p_d = 1$	10.3	38.4	-24	696
current scenario $p_d = 0$	0.10	3.13	-24	235
SESAR scenario $p_d = 1$	0.01	0.67	-8	230
SESAR scenario $p_d = 0$	0.00	0.27	-10	70

Table 4.4: Summary statistics of the difference between the length of the M1 trajectories and the surrogate M3 trajectories. Data refer to the LIRR ACC and are given in kilometers.

## 4.3 Results on Look-Ahead

In this section we investigate the impact of the look-ahead of the controller and its relationship with the shocks. As described in section 1.1, the controller forecasts the trajectories of the flights with a look-ahead which can be tuned. In the most basic setup of the model, this forecast is perfect: the real trajectories coincide with the ones foreseen by the controller. But even the simple setup actually allows some errors from the controllers, or, more precisely, suboptimal decisions. For instance, consider two flights conflicting A and B, as well as a third one C conflicting with B later on. If the controller has a limited time horizon, it can for instance make an action on A to avoid the first conflict, then an action on B or C to avoid the second one. But with an extended time horizon, it could maybe solve both conflicts by making a single action on B. These suboptimal decisions, results of local optimizations rather than a more global one taking into account the whole picture, have nothing to do with an incorrect forecast, in the sense that even the highest precision on trajectories cannot preclude this kind of situation.

On the other hand, and obviously, wrong forecast is another potential source of suboptimal decisions. For instance, a decision can be taken based on the belief that a conflict would appear in the future, whereas it will not actually take place because the computation of the position of the flight was incorrect, because of finite precision of instruments, unforeseen events, etc.

In the following, we investigate both effects by varying the look-ahead of the controller. In order to have incorrect forecast, we use two sources of stochasticity:

- the shocks themselves,
- a special procedure which fools the controller by adding a noise on the velocity of the flights during its forecast.

These two features have been described in details in section 1, see Shocks Module and Velocity Noise Module, respectively.

We begin with the velocity noise, which will turn out to be much less informative than the other one.

### 4.3.1 Velocity Noise

In this experiment, we simply sweep the velocity noise for standard values of parameters: look-ahead of 20 minutes without shocks. We use the LIRR ACC with around 1600 flights.

Figure 4.16 shows the evolution of the number of actions when the noise increases. As one can see, the number of actions does not change much with the noise, especially at the beginning. In fact, we needed to push the noise as far as 50% to see any effect. Even with nearly 100% of noise, the number of actions changes merely by 3%. We do not have a clear explanation as of why this effect is so small. One possible explanation might be that most of the actions of the controllers are actually changes of altitudes. Hence, even if the controller were wrong about the speed of two possibly colliding flights, then both of them are already on different flight levels and thus do not yield additional conflicts. This explanation stands only if there is no “conflict cascade” in the system, i.e. a resolution of conflict leading to another conflict and so on. Even though we did not investigate this point in detail, we think that cascades are rare in the system with the number of flights considered.

Given this negative result, we decided not to use this noise on velocity to destroy the forecast of the controller. Instead, we use the shocks as a source of stochasticity in the following.

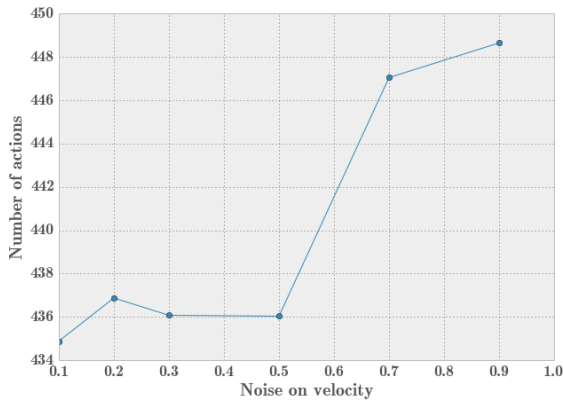


Figure 4.16: Evolution of the number of actions of the controllers with the noise on velocity

### 4.3.2 Look-Ahead and Shocks

In the following we use the shocks to simulate some prototypical weather events, see section 2.1.1. Given the input from validation experts, we decided to use shocks of 20 nautical miles in diameter during two hours. These are big weather events happening mainly in winter time.

Note that in the model, the shocks appear only on 1 FL in height. Since we operate between FL240 and FL350, it means roughly that we need 10 shocks to block a whole column of air of diameter 20 nautical miles. To simulate pretty severe conditions, we thus sweep the number of shocks happening in day from 0 to 1000. For this last value, approximatively 100 weather events blocking a whole column of air happen per day, which represent pretty harsh conditions.

At the same time, we sweep the value of the time horizon. Since we want to discuss scenarios in which the controlled airspaces are much bigger than the current sectors, we go up to one hour for the look-ahead. With this value, we simulate some kind of strategic/tactical planning able to maintain consistency in the decision of the controller on a large area.

We begin with a simple setup with a look-ahead of 20 minutes by sweeping the number of shocks. Figure 4.17 shows the evolution of the number of actions. The evolution is remarkably linear with the number of shocks. This denotes the facility of the algorithm to avoid cascades of conflicts, which would be signed by a super-linear behaviour.

The effect is also important in absolute magnitude. Even with only 200 shocks, the number of actions is increased by more than 20%.

Note that the increase of the number of actions has two sources here. The first one is obviously that the controller needs to avoid forbidden pieces of airspace. But since the controller is blind to future shocks, a second effect is that it makes suboptimal decisions on the re-routings and changes of altitudes of flights. These decision based on a given state can be obsolete if a shock appears in the next time step at a problematic spot. For this reason, we study the interaction of these shocks with the look-ahead.

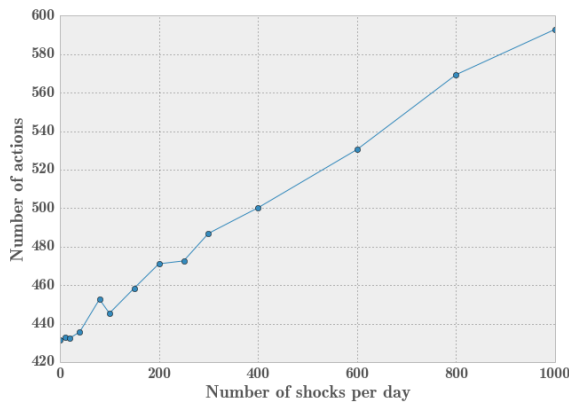


Figure 4.17: Number of actions of the controller for different number of shocks happening in the area.

#### 4.3.2.1 Unrectified trajectories

We begin with the evolution of the number of changes of altitude and the number of re-routed flights. Figure 4.18 shows the result of the procedure for these two metrics. While the first one decreases with the look-ahead the second one actually increases. This is due to the fact that at short times the controller has some difficulties finding a good rerouting because a big angle of deviation would be needed. Hence, it always chooses a change of altitude in this case. For longer time horizons, the controller is able to foresee the conflict and can give a rerouting with a small angle of deviation. This is strikingly similar to reality when controllers use the changes of altitude as measures of emergency.

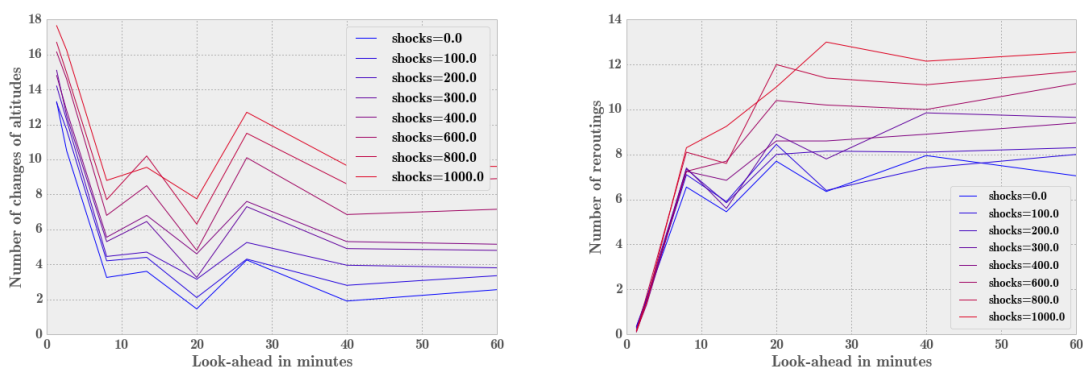


Figure 4.18: Evolution of the number of changes of altitude (left) and number of reroutings (right) as a function of the look-ahead for different number of shocks in the current scenario (unrectified trajectories).

Note also that the effect of shocks seems quite linear for all values of the look-ahead, however with a stronger effect after 5 minutes.

Another interesting feature is the spatial heterogeneity of the actions taken. Figure 4.19 shows different situations in which the look-ahead is set to low or high as well as the number of shocks.

Here we display only the localization of the changes of altitude. The look-ahead has a striking effect on the spatial localisation when there is no shock. From a situation where the actions are quite spread spatially, we go to a situation where there are only a dozen of points which are concentrating all the actions. Interestingly, these points seem also to be adequately spread in the airspace, thus avoiding some unwanted clustering effect.

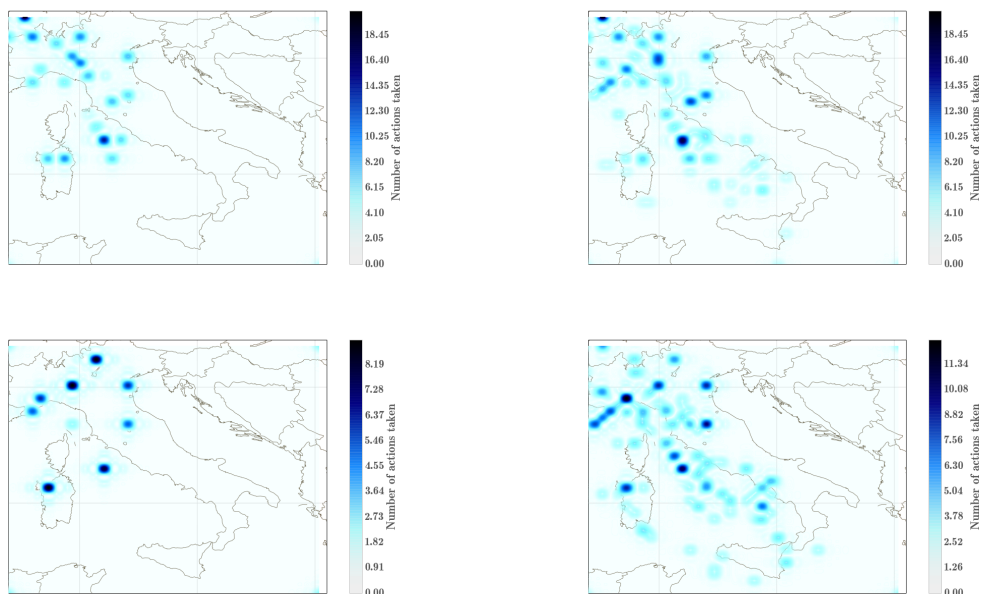


Figure 4.19: Spatial locations of the actions taken by the controller (only changes of altitude). Left panels: low number of shocks. Right panels: high number of shocks. Top: low look-ahead. Bottom: high look-ahead. The figures have been obtained with 10 tactical simulations for 2 strategic simulations. The number displayed are the sum of the actions taken in the 20 simulations. The contours have been smoothed out with cubic spline interpolation to facilitate the reading.

This result is important because in reality it might be easier for controllers to concentrate their actions on a few regions of space – up to a certain point – instead of modifying trajectories all over the airspace. This result would thus be useful to redesign the airspace in the intention of integrating sectors into bigger entities, which would of course need a better time horizon. In this kind of “pre-SESAR scenario”, the choice of the crucial pieces of airspaces which would still require some monitoring could be guided by such analysis.

We see also on the right panels that this structure can be totally destroyed by unforeseen events like shocks. Indeed, if the two top panels are not very different from each other, the two at the bottom display significant differences. Indeed, the right bottom panel do not show a few points concentrating all the actions, but rather a cloud of actions taking place all over the airspace, as in the top panels. Interestingly, this plot seems to display an even more uniform pattern than the top ones, hence displaying the effect of the extended look-ahead too: the fact that different parts of the airspace are used in a more balanced way.

#### 4.3.2.2 Heterogeneity

These results call for a more systematic approach of the spatial heterogeneity. In order to do this, we create a grid of size  $N \times N$  on which we count occurrences of the actions. Hence, we have a matrix of occurrences for which each entry is the number of actions made by the controller in the corresponding 2-D region. We then compute the standard deviation on all the matrix, divided by the average. This gives an indication of how spread are the actions in the airspace. Note that a complementary measure could have been something like the upper decile over the average. However, due to the high number of null values in the matrix, quantile-based metrics are not very informative.

On figures 4.20 and 4.21 we show the evolution of the heterogeneity for changes of altitude and reroutings with respect to shocks and look-ahead. The effect of shocks is straightforward: the higher the frequency of shocks, the more homogeneously spread are the actions taken by the controller, both with changes of altitudes and reroutings. This is due to the fact that the controller is blind to shocks and needs to take late actions to avoid these unforeseen events.

The effect of the look-ahead seems to be quite the same in most cases. This might be due to the fact that there could be few dangerous spots in the area, and with a short time horizon the controller needs to take action right at these points. When the look-ahead increases, the actions can be taken sooner and thus are more spread in the area. Note that interestingly in the case where there is no shock, the heterogeneity of the changes of altitude seems to increase with the look-ahead. Indeed, it could be due to the fact that without shocks, the trajectories can be perfectly forecast and thus the actions take place exactly at the entrance of the airspace. The entrance points are quite localized, so the heterogeneity increases.

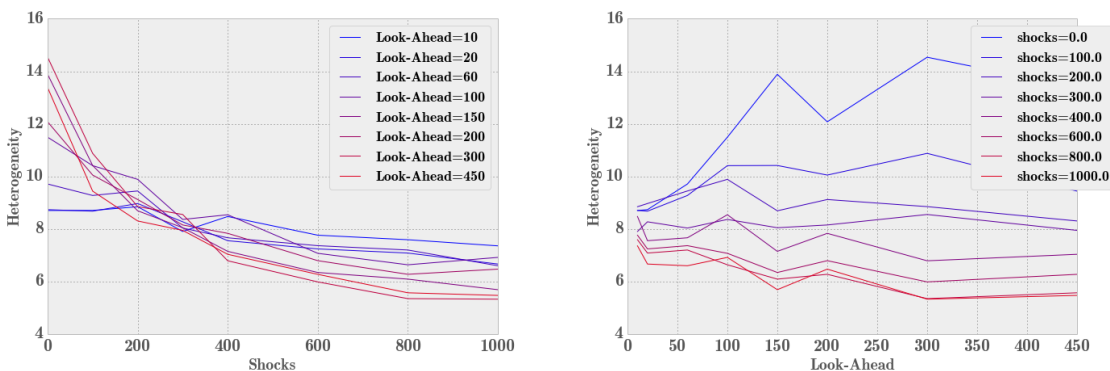


Figure 4.20: Heterogeneity of the changes of altitude as a function of the number of shocks (left) and the look-ahead (right).

Finally, note also that changing the parameter  $N$  (the grid's resolution) in the analysis does not modify qualitatively the results.

#### 4.3.2.3 Rectified trajectories

In order to predict the effect of an extended look-ahead in the SESAR scenario, we do the same experiments with the (fully) rectified trajectories, by sweeping the number of shocks and the value of the look-ahead. Some results are displayed in figure 4.22. The general trend is the same than previously for the changes of altitude, but the number of reroutings is just too small to make any statistics. Thus, it seems that the controller is able to solve nearly every conflict just with a change of altitude.

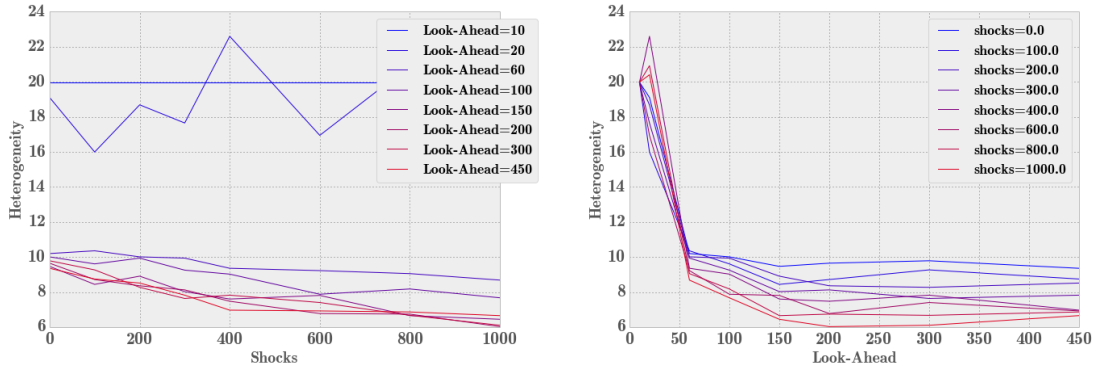


Figure 4.21: Heterogeneity of the reroutings as a function of the number of shocks (left) and the look-ahead (right).

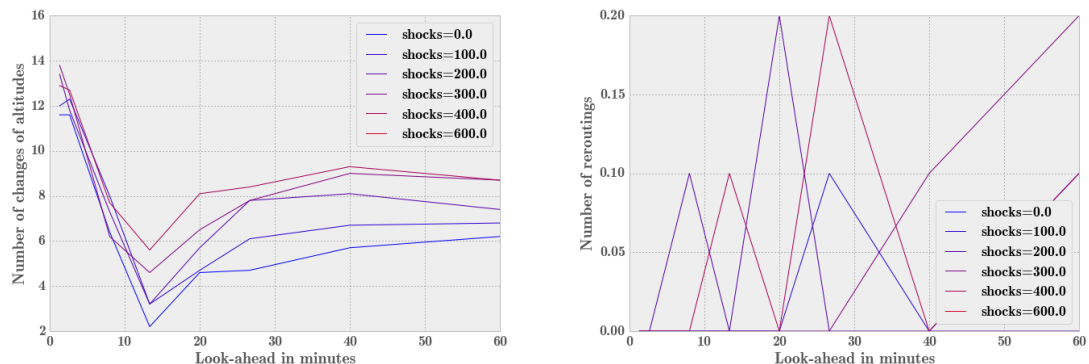


Figure 4.22: Evolution of the number of changes of altitude (left) and reroutings (right) as a function of the look-ahead and the number of shocks in the SESAR scenario (straight trajectories).

The spatial heterogeneity is also interesting to study in the case of rectified trajectories. In figure 4.23 we present the results of different scenarios. The pictures are essentially the same than in the current scenario, with unrectified trajectories, even though the actions seem to be more concentrated here. The shocks spread the actions spatially, whereas the look-ahead seems to increase the heterogeneity.

Figures 4.24 and 4.25 show some more quantitative measurements of these effects. The effect of shocks is essentially the same, which is the homogenization of the actions. The effect of the look-ahead seems a bit different. For the changes of altitude, a low level of shock imply that the heterogeneity is increasing with the look-ahead, which is similar to the effect we saw for unrectified trajectories. When the frequency of the shocks increases, the heterogeneity increases sharply around ten minutes then decreases slowly. This non-monotonic effect is non-trivial we provide the following possible explanation. When the look-ahead is very small, the controller reacts at the last moment and thus at some random locations when there are shocks. Then the controller is able to forecast

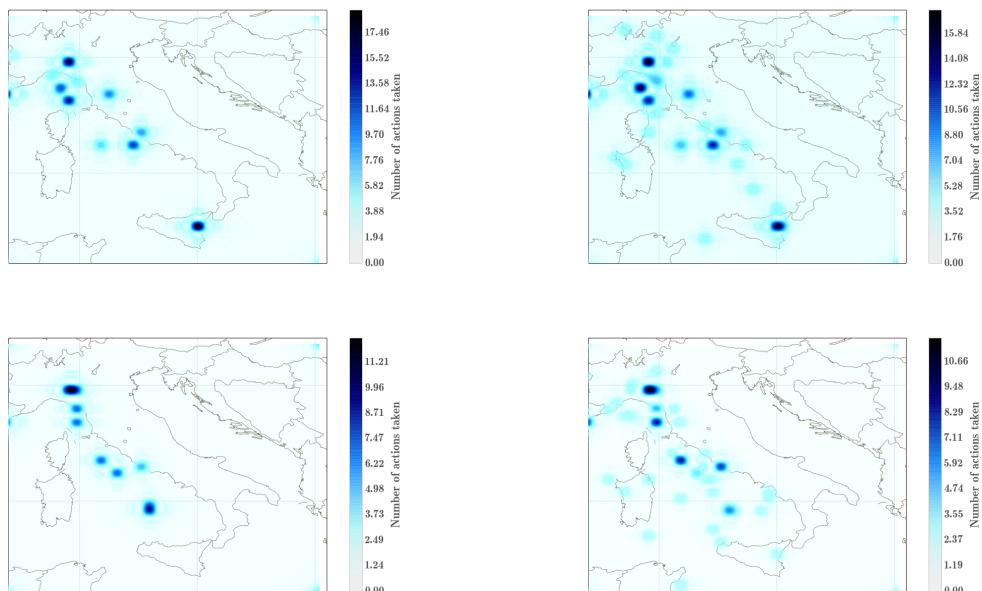


Figure 4.23: Spatial locations of the actions taken by the controller (only changes of altitude) in the SESAR scenario. Left panels: low number of shocks. Right panels: high number of shocks (400). Top: low look-ahead. Bottom: high look-ahead. The figures have been obtained with 10 tactical simulations for 1 strategic simulation. The number displayed are the sum of the actions taken in the 10 simulations. The contours have been smoothed out with cubic spline interpolation to facilitate the reading.

better the trajectory and the actions take place closer to the entrance. But when the look-ahead is too high, the controller takes too many useless actions due to unforeseen events: some of them are very close to the entrance, others at located at some random points, and the heterogeneity decreases again.

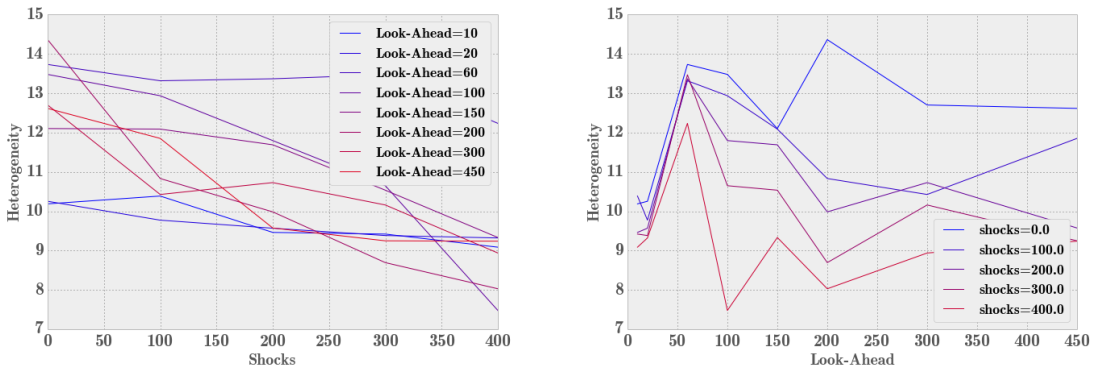


Figure 4.24: Heterogeneity of the changes of altitude as a function of the number of shocks (left) and the look-ahead (right) in the SESAR scenario.

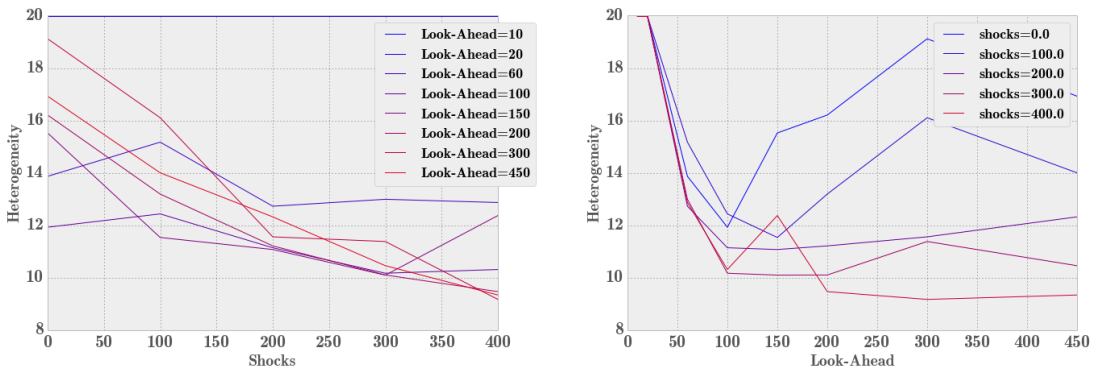


Figure 4.25: Heterogeneity of the reroutings as a function of the number of shocks (left) and the look-ahead (right) in the SESAR scenario.

The heterogeneity of the reroutings exhibits also a non-trivial pattern, which is strongly related to the other one. Essentially, it is the same pattern, except for the initial heterogeneity at very low look-ahead. The difference here is that, as already stated before, the controller uses only the changes of altitude when the look-ahead is small. Hence, there are only few reroutings, which are naturally very concentrated.

### 4.3.3 M1 Capacities

### 4.3.3.1 Unrectified trajectories

In this section, we investigate the impact of the presence of capacities on the controller's action. More precisely, we study the impact of M1 capacities, in the sense that the traffic of the strategic phase has to be compliant with some capacities, whereas the traffic in the tactical phase do not take into account any capacities in the decision making, see section 4.4 for this kind of experiments.

The experiments we conducted are made with LIRR, with a constant time horizon, no shock and no direct. We set a number of flights as input for the strategic model, and then we change the capacities in various ways.

- In the first experiment, we decrease uniformly the capacities of all sectors.
- In the second one, we impair severely three central sectors, increasing the capacities of the surrounding sectors to have the same average capacity. Then we decrease all capacities uniformly like in the previous point.
- The last one is the witness in which we remove the capacity constraint and change the number of flights submitting a flight plan.

We make 100 iterations on the tactical model for each 10 strategic simulations.

The results are presented in figure 4.26. We display on the same graph the relationship between the number of actions and the number of flights actually flying during the tactical phase, for all experiments. The results for the witness (in red) is straightforward and consistent with the scaling found in section 4.1. Indeed, a least-square regression with the function  $bx^a$  yields the following values:  $a = 2.0 \pm 9.10^{-5}$  and  $b = 8.410^{-5} \pm 3.10^{-11}$ , i.e. a pure quadratic law. We recall that the reason behind this scaling is simply that the potential conflicts are scaling as the number of pairs, i.e. quadratically with the number of flights.

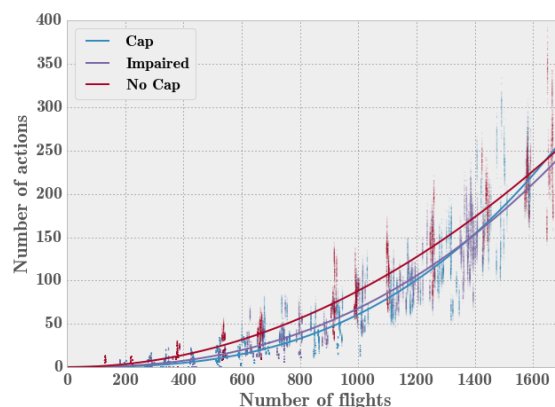


Figure 4.26: Different scaling for different scenarios. The scatter plots have been obtained with a uniform reduction of the capacities (light blue), with some sectors severely impaired (violet) and without any capacity (red). The solid lines are the result of linear power law regressions for each set of data.

Interestingly, the regression for the two other experiments yield another scaling. With the same regression, the violet line yields:  $a = 2.4 \pm 1.10^{-4}$  and  $b = 3.610^{-6} \pm 8.10^{-14}$  and the blue line one gives:  $a = 2.75 \pm 2.10^{-4}$  and  $b = 3.410^{-7} \pm 1.10^{-15}$ . In other words, they are clearly displaying super-quadratic behaviors. But before explaining why, we comment on the fact that despite this

behavior, these two cases usually need less actions than the capacity-free case for the same number of flights. This is due to the fact that capacities tend to spread the flights during the day. Hence the time concentration of flights decreases during peaks, which decreases the number of potential conflicts (flights are flying at different times).

The same argument explains the super-quadratic behavior. Indeed, due to our experimental procedure, when the number of flights increases, it means that the capacities are less binding, since we keep the number of flights fixed as input to the strategic layer. Hence, when the number of flights increases, the number of potential conflicts increases more quickly than  $x^2$ , because more flights are flying at similar times.

#### 4.3.3.2 Rectified trajectories

In order to predict the effect of capacities in the case where the trajectories are straight, we make the same kind of experiment with rectified trajectories. On figure 4.27 we show the equivalent of figure 4.26 computed for rectified trajectories. Since the cases where the the capacities of some of the sectors have been decreases and the normal case (with capacities) are sensibly the same, we do not display the former on the plot.

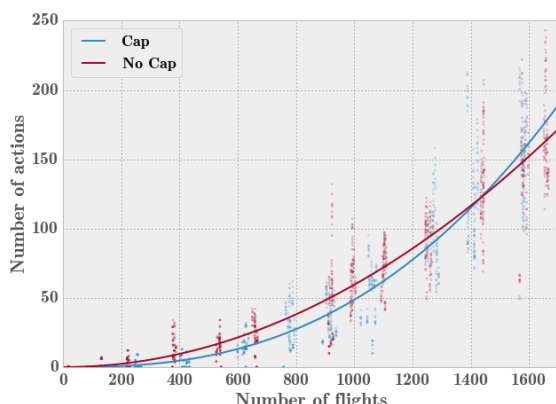


Figure 4.27: Different scaling in different scenarios for the number of actions as a function of the number of flights in the area in the case of straight trajectories. In red, the simulations were done without capacities. If blue, constant capacities were applied.

What we find is that the “free” case – without capacities – still displays a pure quadratic scaling. Similarly, when the capacities are binding, the scaling is super linear with an exponent close to 2.5 as in the unrectified case. The pre-factor are obviously smaller than in the unrectified case too (less number of actions overall). Their respective values between the free and constrained case are also the sensibly the same, which means that, once again, the introduction of capacities leads to a reduction of the number of actions for a given number of flights. The only possible difference might be in the super-quadratic behavior of the free case seems to kick at a smaller number of flights that in the undirected case. Since means that quickly the introduction of capacities could lead to a higher number of actions, since the curves cross. It is not clear though if this results is statistically relevant or note.

## 4.4 Results on the Multi-sector ABM

In this section we describe some results obtained by using the multi-sector module of section 1.2.9, the rectification procedure of section 1.3.2 and the Conflict-Free Flight Plan Generator of section 3.2. In particular, we considered the LIRR ACC that involves 10 ATC sectors with capacities 41, 30, 24, 20, 18, 18, 17, 17, 16, 15, whose boundaries are shown in Fig. 4.28. We recall that the efficiency of LIRR in the current scenario is  $E = 0.945$ .

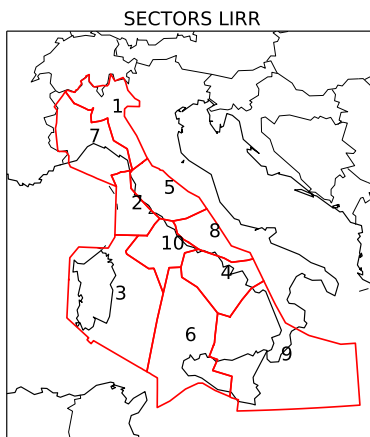


Figure 4.28: Sectors in the italian LIRR ACC.

Here we are starting from M1 flight plans relative to the current scenario and with  $p_d = 1$ . When applying the ABM without using the multi-sector module, see section 4.2, we obtained M3 surrogate files with efficiency  $E = 0.967$ , see Fig. 4.8.

In Fig. 4.29 we show the impact of directs in determining the efficiency of the surrogate M3 trajectories as a function of the sectors' capacity. In fact, we start from the sectors' capacities inferred from real data and the flight planes (M1 files) released by considering such capacities for the  $N_f = 2122$  aircraft present in the ACC. After such flight plans are released, we then change the sectors' capacity by a factor  $x$  ranging from 0 to 1.5 and check how this affects the fact that directs are issued or not. Since directs are one major strategies to rectify trajectories, we thus have the possibility of checking how capacity affects rectification, leaving any other parameter unaltered. For example, the choice  $x = 0$  does not mean that no aircraft can be present in the sector. It simply means that no direct from other sectors is accepted. All aircraft that were supposed to be in the sector according to the planned flight plan, will still be flying within that sector. The case  $x = 1$  corresponds to the capacities inferred from real data. Interestingly, when  $x > 1$  we do not observe any improvement of the efficiency, while efficiency decreases with  $x$ , i.e. for decreasing capacities. Our interpretation is that real capacities are chosen high enough as to ensure reasonable margins to the ATC controllers for managing safely risky situations. Finally, it is worth noticing that the plateaus value observed for  $x > 1$  is compatible with the efficiency value  $E = 0.967$  obtained in section 4.2 for the surrogate M3 flight trajectories, within the error bars.

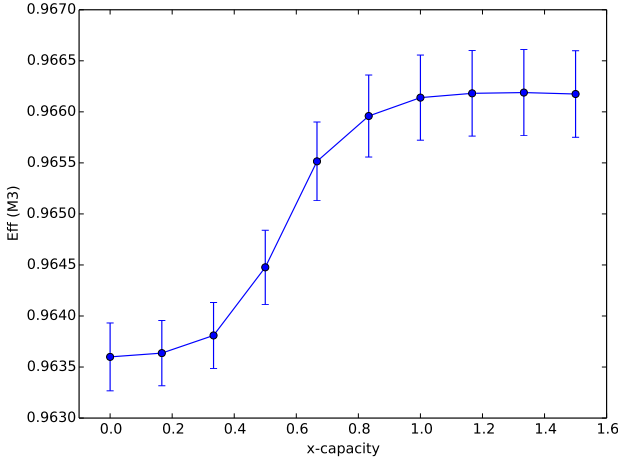


Figure 4.29: Efficiency of the surrogate M3 trajectories as a function of the sectors capacity.

Let us now investigate what is the role of sectors' capacity in the presence of shocks. In the simulations we present below we have shocks with a duration  $D_S$  uniformly distributed in the range [5, 120] min and with centers  $C_S$  uniformly distributed all over the ACC. In the simulations we will show below, the directs module is disabled and we do not artificially inject delays in the flight departing times. This is done in order to isolate the effects genuinely due to conflicts and shocks.

In Fig. 4.30, for the 10 LIRR sectors we show the quantity:

$$\overline{EX} = \sum_{j=1}^{24} |O_j^{M1} - O_j^{M3}| \quad (4.2)$$

where  $O_j^{M1}$  is the number of aircraft in the  $j$ -th hourly time window as observed in the planned trajectories and  $O_j^{M3}$  is the same quantity for the simulated trajectories. The figure is a scatter-plot showing  $\overline{EX}$  for the current (vertical axis) and SESAR scenario (horizontal axis). The values shown are averages performed over 1000 simulations. The color code indicates the 8 considered values for the average number of shocks per time-step per flight-level  $S_m$ . In all cases except Sector 2 and Sector 5, we have that the points are above the first diagonal of the plot, thus indicating that on average the SESAR scenario performs better than the current scenario.

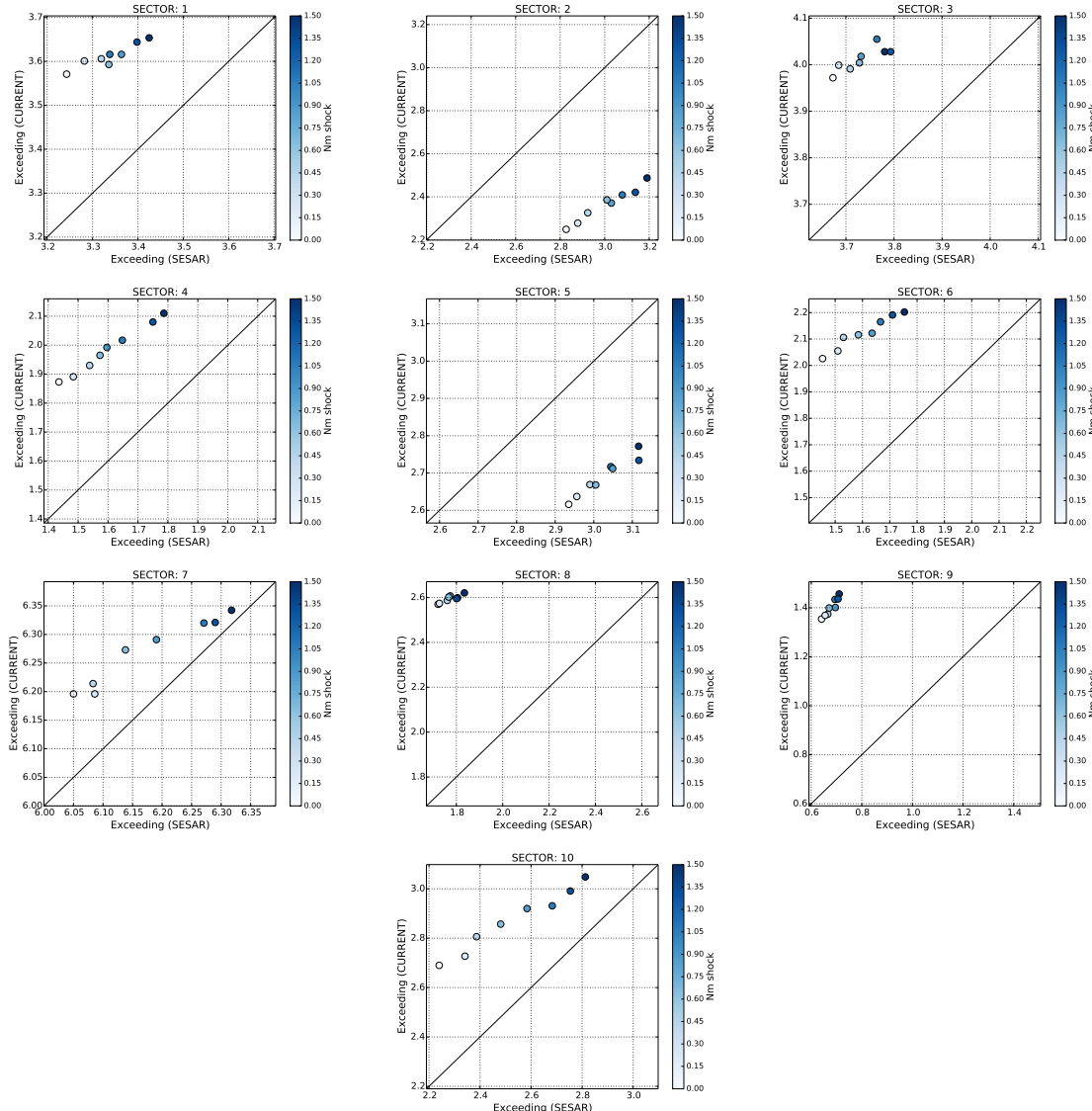


Figure 4.30: Scatter-plot showing  $\overline{EX}$  defined in Eq. 4.2 for the current (vertical axis) and SESAR scenario (horizontal axis). The values shown are averages performed over 1000 simulations. The color code indicates the 8 considered values for the average number of shocks per time-step per flight-level  $S_m$ .

The  $\overline{EX}$  metric directly measures the differences between the sectors occupancy in the M3 and M1 files, assumed that the capacity is the same in the two cases. Therefore, under this assumption, this metric measures the occupancy performances independently from the capacity. The absolute value is introduced in order to evaluate in a negative way any discrepancy between planned and realized occupancy, as a proxy of the robustness of the system with respect to occupancy. In fact, even if the actual occupancy of a certain sector is smaller than what was planned, this might result in a larger occupancy in adjacent sectors or in other hourly time windows and having destabilizing effects on the system.

In order to better illustrate the behavior of the  $\overline{EX}$  metrics, in Fig. 4.31 we show the sectors occupancy over the 24 hours for a specific value of the number of shocks  $S_m = 1.5$  for the current and the SESAR scenario. The data shown refer to a single specific simulation. When red is visible this indicates that occupancy in the M1 files is larger than in the M3 files. The opposite when yellow is visible. Orange indicates that occupancy in the planned trajectories equals occupancy in the simulated trajectories. In the left panels we show the results relative to the current scenario, while in the right panels we show the results for the SESAR scenario. The times at which occupancy approaches or exceeds capacity are always located during daylight hours. The top panels refer to Sector 2 and they illustrate a situation when the flight trajectories were correctly planned in the current scenario and incorrectly planned in the SESAR scenario, where the M1 files occupancy exceeds capacity. In this case we have  $\overline{EX} = 6$  in the current scenario and  $\overline{EX} = 3$  in the SESAR scenario, meaning that for this specific simulation the SESAR scenario performs better than the current one in terms of occupancy's predictability. From Fig. 4.30 we however know that in this sector the current scenario performs better than the SESAR scenario, on average. The central panels refer to Sector 5 and they illustrate a situation when the flight trajectories were correctly planned both in the current scenario and in the SESAR scenario. However, in this case we have  $\overline{EX} = 4$  in the current scenario and  $\overline{EX} = 6$  in the SESAR scenario, meaning that for this specific simulation the SESAR scenario performs worse than the current one in terms of occupancy's predictability, in line with the results of Fig. 4.30. Finally, the bottom panels refer to Sector 9 and illustrate a situation in which we are clearly far away from the capacity threshold. In this case the current scenario performs well in terms of occupancy predictability (e.g.  $\overline{EX} = 0$ ), while we have  $\overline{EX} = 1$  in the SESAR scenario, even though capacity is not exceeded.

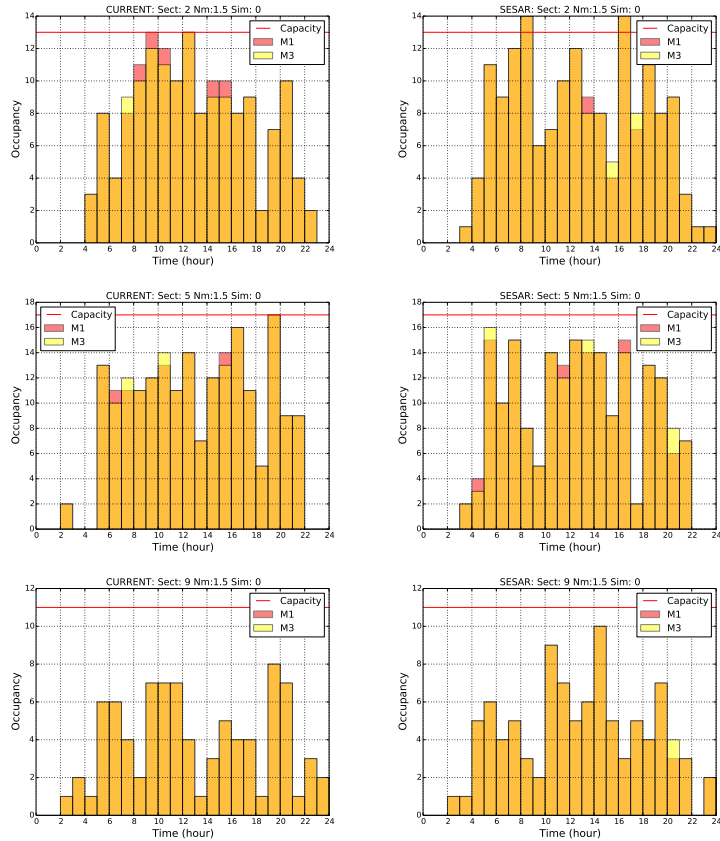


Figure 4.31: Sectors occupancy over the 24 hours for a specific value of the number of shocks  $S_m = 1.071$  for the current and the SESAR scenario. When red is visible this indicates that occupancy in the M1 files is larger than in the M3 files. The opposite when yellow is visible. Orange indicates that occupancy in the planned trajectories equals capacity in the simulated trajectories. In the left panels we show the results relative to the current scenario, while in the right panels we show the results for the SESAR scenario.

In Fig. 4.32 we show the number of re-routings (blue line) and number of flight-levels (green line) for the current (left panel) and SESAR (right panel) scenario as a function of the number of shocks  $S_m$ . In all cases there is a linear dependence from  $S_m$ . Our interpretation is that this is due to the fact that shocks are uniformly distributed within the ACC in the present simulations.

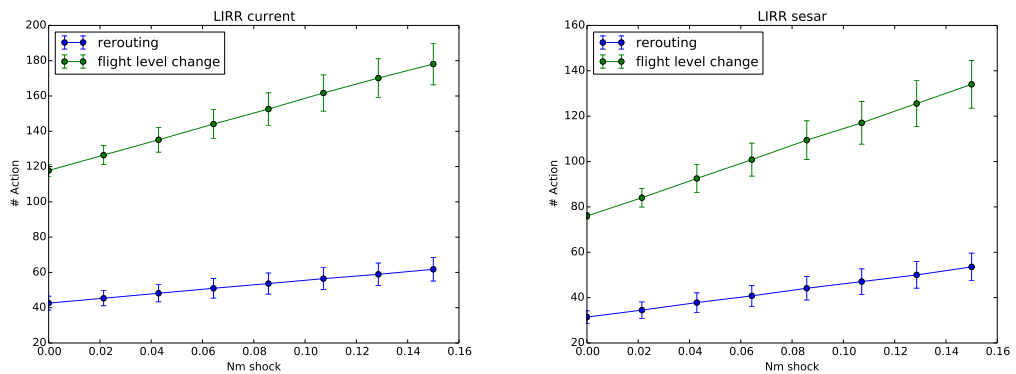


Figure 4.32: Number of re-routings (blue line) and Number of flight-levels (green line) for the current (left panel) and SESAR (right panel) scenario as a function of the number of shocks  $S_m$ . The error-bar of the first point in the central panels is very small as it was obtained for simulations without shocks and therefore quite stable.

## 4.5 Validation of results and identification of operational benefits

The results of the analyses carried out in the current and SESAR scenarios have been validated with the support of ATM expert Dr. Fedja Netjasov from University of Belgrade. The objective of this activity was the identification of the main operational benefits envisaged from the analyses' results. The results obtained cover, implicitly or explicitly, all four main SESAR benefits: Environment, Cost-Effectiveness, Capacity and Safety. In particular the following operational benefits can be identified:

- Safety improvement from the reduction of total number of conflicts and reduction of controller workload: controller's activity in the SESAR scenario will change, moving from a situation where he has to give attention to an high number of conflicts concentrated in specific points to a situation where he will have to manage less conflicts spread in a much larger portion of the airspace. This will imply a quantitative and qualitative change of controller workload. Quantitative in a sense that total workload will be reduced while qualitative in the sense that nature of controllers tasks will be changed (shifting from mainly conflict resolution to mainly traffic monitoring tasks).
- Reduction of environmental impact and system costs reduction: results presented in section 4.2 show that rectifying trajectories is beneficial for the general efficiency of the system. In addition sector throughput (traffic load) in SESAR scenario is mostly lower than sector capacity (see Figures 4.30 and 4.31) due to the fact that traffic is spread around the airspace leading to more balanced traffic load among sectors.
- Improved airspace management: results related to the scenario where controllers have an increased look-ahead show that in SESAR scenario this increase will have the consequence of shifting workload from Executive air traffic controller (EC) to Planning air traffic controller (PC), i.e. EC will have lower workload due to more monitoring tasks and less conflict resolution and separation assurance tasks. Given that controller have a tool to monitor the traffic (e.g. Medium Term Conflict Detection), all the actions could be taken at the entrance of the airspace. This could lead to a standard procedure where pilots systematically receive instructions at the entrance of a controlled area and then fly free.
- Capacity definition and predictability: from most of the analyses carried out it emerged that the definition of capacity in the SESAR scenario will have to take into account the shifting of the controller workload from mainly conflict resolution to mainly monitoring tasks. In the SESAR scenario it also foreseen a reduction of the capacity infringements and an increased predictability of the infringements.

## FINAL REMARKS

In this document we have illustrated the empirically grounded agent based model for the SESAR scenario developed within the WP-E research project ELSA.

Chapter 1 was devoted to the description of the model, Chapter 2 illustrated the main activities performed for the calibration of some model parameter and the validation of the main model's assumptions. Chapter 4 was devoted to an illustration of some results obtained with the model. We performed simulations with the aim of showing how the different modules of the model can work. Therefore, the results illustrated in this section must be intended as indicative of the models capabilities.

One of the main results obtained in section 4.1 was that the number of operations performed by the controller scales with  $N_f^2$ , where  $N_f$  is the number of aircraft present in the sector, see Fig. 4.3. Moreover, Fig. 4.6 indicates that given the number of possible conflicts as desired from the M1 files, the average number of operations that a controller has to perform in order to avoid conflicts can be predicted in terms of a linear law. Specifically, the figure shows the existence of two different linear regimes. For values of efficiency close to unity the curve can be fitted with a linear relationship whose slope is of the order of 0.05, while for lower values of efficiency we have a linear relationship whose slope is of the order of 0.01. Finally, Fig. 4.7 indicates that the number of possible conflicts in the SESAR scenario is predicted to be more spread all over the considered ACC, rather than concentrated in specific points as in the current scenario. This might explain why on average we expect a smaller number of operations to be performed by the controls in the SESAR scenario with respect to the current scenario, see again Fig. 4.1.

The investigations performed in section 4.2 on different ACCs confirm the expectation of a smaller number of operations to be performed by the controls in the SESAR scenario. However, we were not able to find any universal law able to describe the behavior of different ACCs in a unified way. This would then imply that the specific details of an ACC (geographic area, number of aircraft, structure of the current scenario navigation point network) play an important role. One possible common feature between the different ACCs is that the distribution of number of reroutings for the vast majority (35 out of 39) of the ACCs seems to follow a Gaussian distribution when the issuing of directs is allowed, while this no longer true when directs are not allowed. The importance of this issue lies in the fact that the gaussianity ensures that on average the probability that a controller performs a large number of operations remains low.

In section 4.3 we mainly investigated what is the role of having a larger look-ahead in the management of the conflicts. Fig. 4.22 shows that indeed enlarging the look-ahead brings a decrease in the number of the operations that the controller has to do. Moreover, after a certain time horizon of about 25 minutes the number of reroutings seems to be independent of the average number of shocked areas. It is also interesting to compare the spatial distribution of shocks when there is a high number of shocks and a low look-ahead (top-right panel of Fig. 4.23) and a high number of shocks and a large look-ahead (bottom-right panel of Fig. 4.23). The two mentioned panels indicate that indeed with a larger look-ahead the management of the trajectories improves drastically. Fur-

thermore, a comparison between Fig. 4.19 and Fig. 4.23 indicates that in the SESAR scenario there is an overall better management of the trajectories with respect to the current scenario.

In section 4.4 we investigated the capabilities offered by the implementation of sectors within the ACC. In the present version of the model, although the existence of sectors inside the ACC is permitted, the air traffic management is still uniform, meaning that we have controllers that behave in the same way within the ACC. This is done in view of the fact that at the level of ACC there is a certain uniformity of behavior amongst the controllers of different sectors, also due to the fact that they are all working in the same physical place. This also contributes to have a lower level of coordination amongst controller, with respect to the case of controllers working on sectors belonging to different ACCs. One of the main results of this section is that in the SESAR scenario the sectors' occupancy exceeds capacity in a smaller number of cases and for less time, as can be seen by comparing the results of Fig. 4.30 and Fig. 4.31. It should be emphasized that the way we incorporate capacity constraints into the model is not fully satisfactory. In fact, when generating flight plans with larger efficiency, the capacity constraints will not be modified. Therefore we have an hybrid situation where we consider flight plans with enhanced efficiency and with capacity constraints that are still those of the current scenario.

The model we have described in this document has one main feature which to a certain extent might also be its limitation: it is a simple model. In fact, the interaction between aircraft is managed in a deterministic way. This simple agent based model do not implement learning mechanisms [11] or specific fitness measures besides the fact that in the conflict resolution module we follow the shortest trajectory amongst the possible ones.

Having that, we see two main possible ways for further research starting from this model.

**1** - On one side we might maintain the model as simple as it is and try to use it in order to study specific problems related to the air traffic management in the current and SESAR scenario. Examples might include (i) the study of the resilience of the ATM system after a major shock occurs or (ii) the study of the optimal conflict resolution in the presence of high levels of traffic concentrated in small areas or (iii) the detection or recurrent patterns used by the controllers to solve conflicts. In other words the idea is to use the current version of the model in order to formulate empirically grounded numerical null hypothesis for the study of specific problems.

**2.a** - On the other side we might explore the possibility of augmenting our model capabilities by implementing learning and self-adaptation mechanisms as well as some level of intelligence for the agents. It is worth mentioning that a preliminary attempt in this direction was already done in deliverable D2.3 [1], where we had introduced a velocity change module that was used as a conflict resolution tool. The intelligence amongst agents might also be used in order to model a sort of self-organization amongst aircraft in order to mimic a scenario in which aircraft pilots, each endowed with a set of policy rules fulfilling some airline constraints, will perform an *active* conflict resolution at a tactical level.

**2.b** - Another point worth of further investigation would be to consider the possibility of implementing a conflict-resolution module providing conflict-free trajectories optimized at a global level. This would however imply a complete revision of the philosophy underlying this model.

## Bibliography

- [1] ELSA project, *E.02.18-ELSA D2.3 Calibrated agent-based model – final draft*, Version: 24/02/2014, (Restricted audience)
- [2] A. Agogino, K. Tumer. Regulating Air Traffic Flow with Coupled Agents. In: Proceedings of 7<sup>th</sup> Int. Conf. on Autonomous Agents and Multiagent Systems (AAMAS 2008). (Estoril, 12-16 May 2008, Portugal).
- [3] S. R. Wolfe, P. A. Jarvis, F. Y. Enomoto, M. Sierhuis. A Multi-Agent Simulation of Collaborative Air Traffic Flow Management. In: Edited Collection on Multi-Agent Systems for Traffic and Transportation (2009).
- [4] B. W. Kernighan; D. M. Ritchie. *The C Programming Language*. (Prentice Hall, England, 1988).
- [5] G Van Rossum; Fred L. Drake Jr *Python reference manual* (Centrum voor Wiskunde en Informatica, Netherlands, 1995)
- [6] Smart, W. M. *Text-Book on Spherical Astronomy*, 6th ed. Cambridge, England: Cambridge University Press, p. 18, 1960.
- [7] David E. Goldberg *Genetic Algorithms in Search, Optimization, and Machine Learning* (Addison-Wesley Professional, 1 edition, 1989)
- [8] ELSA project, *E.02.18-ELSA D1.3 Statistical Regularities in ATM - final draft*, Version: 21/12/2012, (Restricted audience)
- [9] A. Clauset, C. R. Shalizi, M. E. J. Newman, *Power-law distributions in empirical data* SIAM Review, **51**, 661-703, (2009)
- [10] M.A. Stephens *EDF statistics for goodness of fit and some comparisons* J. Am. Stat. Assoc., **69** 730, (1974)
- [11] A. K. Agogino, K. Tumer. *A multiagent approach to managing air traffic flow*. Auton Agent Multi-Agent Syst **24**, 1-25 (2012).